




AgRP neuron cis-regulatory analysis across hunger states reveals that IRF3 mediates leptin's acute effects

Received: 8 December 2023

Accepted: 14 May 2024

Published online: 31 May 2024

 Check for updates

Frankie D. Heyward ^{1,2,3,4,5} ✉, Nan Liu ^{6,7,8}, Christopher Jacobs ^{1,2},
Natalia L. S. Machado ^{3,9}, Rachael Ivison ^{1,2}, Aykut Uner ^{1,3,4},
Harini Srinivasan^{1,2}, Suraj J. Patel^{1,10,11}, Anton Gulko¹, Tyler Sermersheim¹,
Linus Tsai ^{1,2,3} & Evan D. Rosen ^{1,2,3} ✉

AgRP neurons in the arcuate nucleus of the hypothalamus (ARC) coordinate homeostatic changes in appetite associated with fluctuations in food availability and leptin signaling. Identifying the relevant transcriptional regulatory pathways in these neurons has been a priority, yet such attempts have been stymied due to their low abundance and the rich cellular diversity of the ARC. Here we generated AgRP neuron-specific transcriptomic and chromatin accessibility profiles from male mice during three distinct hunger states of satiety, fasting-induced hunger, and leptin-induced hunger suppression. Cis-regulatory analysis of these integrated datasets enabled the identification of 18 putative hunger-promoting and 29 putative hunger-suppressing transcriptional regulators in AgRP neurons, 16 of which were predicted to be transcriptional effectors of leptin. Within our dataset, Interferon regulatory factor 3 (IRF3) emerged as a leading candidate mediator of leptin-induced hunger suppression. Measures of IRF3 activation *in vitro* and *in vivo* reveal an increase in IRF3 nuclear occupancy following leptin administration. Finally, gain- and loss-of-function experiments *in vivo* confirm the role of IRF3 in mediating the acute satiety-evoking effects of leptin in AgRP neurons. Thus, our findings identify IRF3 as a key mediator of the acute hunger-suppressing effects of leptin in AgRP neurons.

Increasing the granularity with which we understand the homeostatic regulation of energy balance (i.e., food intake and energy expenditure) will represent a major step towards the ultimate goal of treating obesity. It has long been recognized that the arcuate nucleus (ARC) of the

hypothalamus is indispensable for maintaining energy homeostasis¹. Amid the rich diversity of cell types within the ARC, AgRP neurons play a critical role in coordinating the physiological processes needed to maintain energy homeostasis in the face of changing energy availability.

¹Division of Endocrinology, Diabetes, and Metabolism, Beth Israel Deaconess Medical Center, Boston, MA, USA. ²Broad Institute of MIT and Harvard, Cambridge, MA, USA. ³Harvard Medical School, Boston, MA, USA. ⁴Center for Hypothalamic Research, Department of Internal Medicine, UT Southwestern Medical Center, Dallas, TX, USA. ⁵Department of Neuroscience, UT Southwestern Medical Center, Dallas, TX, USA. ⁶Cancer and Blood Disorders Center, Dana-Farber Cancer Institute and Boston Children's Hospital, Boston, MA, USA. ⁷Bone Marrow Transplantation Center of the First Affiliated Hospital, Zhejiang University School of Medicine, Hangzhou, China. ⁸Liangzhu Laboratory, Zhejiang University, Hangzhou, China. ⁹Department of Neurology, Beth Israel Deaconess Medical Center, Boston, MA, USA. ¹⁰Division of Gastroenterology & Hepatology, UT Southwestern Medical Center, Dallas, TX, USA. ¹¹Center for Human Nutrition and Department of Internal Medicine, UT Southwestern Medical Center, Dallas, TX, USA. ✉ e-mail: frankie.heyward@UTSouthwestern.edu; erosen@bidmc.harvard.edu

AgRP neurons are activated during states of negative energy balance (i.e., fasting) and selective chemogenetic and optogenetic activation of these neurons drives mice to become markedly hyperphagic¹. Conversely, post-developmental genetic deletion of AgRP neurons renders mice profoundly hypophagic, and during periods of simulated energy repletion, the satiety-evoking adipokine leptin has been shown to decrease the firing rate of AgRP neurons^{2,3}. Finally, CRISPR-Cas9-mediated genetic ablation of the leptin receptor from adult mouse AgRP neurons results in profound obesity that is similar to that exhibited by *db/db* whole-body leptin receptor null mice, indicating that leptin's anti-obesity effects can be mediated via its direct effects on AgRP neurons⁴. Given these findings, much effort has been directed towards elucidating the transcriptional programs that allow AgRP neurons to respond appropriately to changes in energy availability.

Distinct alterations in the transcriptional profiles of AgRP neurons have been noted in response to fasting, including genes encoding neurotransmitter receptors, ion channels, and secreted proteins⁵. These transcriptional changes are suspected to underlie the requisite cell type-specific alterations in neuronal excitability that enable AgRP neurons to influence downstream satiety signaling circuits.

Transcriptional regulation is a key mechanism by which leptin confers its effects on neurons. Mice with a pan-neuronal deletion of signal transducer and activator of transcription 3 (STAT3), the best-known transcriptional effector of leptin action, exhibit profound obesity which is similar to that seen in leptin receptor null mice^{6–8}. Moreover, mice devoid of STAT3 specifically in AgRP neurons exhibit an increase in body weight compared to control mice⁹. Activating transcription factor 3 has also been shown to mediate some of the effects of leptin *in vivo*¹⁰. Additional evidence of a transcriptional basis for leptin comes from the observation that leptin's suppressive effects on AgRP neuronal activity occur gradually over a 3-hour time course, a finding that implicates the involvement of transcriptional regulation³.

Previous studies have characterized the transcriptional events that occur in all leptin-receptor-expressing cells in the hypothalamus in response to leptin^{10,11}. More recently, one group assessed AgRP neuron-specific transcriptional changes in response to fasting and leptin-administration, observing 33 leptin-induced transcriptional changes that were linked to biological processes suspected to facilitate behavioral changes in response to fluctuations in energy availability¹². Another group generated a chromatin accessibility landscape of the broad population of leptin receptor-expressing cell types in the brain, yet no bioinformatic assessment of leptin-induced changes in the epigenetic landscape was offered¹³. To date, we lack a rich and comprehensive understanding of the transcriptional and transcriptional regulatory changes that occur in AgRP neurons in response to leptin.

High throughput DNA sequencing techniques that generate genome-wide profiles of open chromatin regions (OCRs) have been used to infer the identity of transcription factors (TFs) that govern the cellular identity and activity state of a variety of cell-types^{14–18}. However, applying this approach to study transcriptional regulation within purified populations of AgRP neurons has been challenging for two reasons. The first has to do with the rich cellular heterogeneity within the ARC, where over 50 cell-types have been identified, which necessitates the isolation of these cells prior to their being studied¹¹. The second is owed to the relatively low abundance of mouse AgRP neurons (~9000 per mouse)¹⁹ compared to the cellular input typically required for traditional deeply sequenced genomic profiling techniques ($\geq 100,000$). To surmount these two obstacles, we developed mouse lines in which AgRP neurons express tagged ribosomes and nuclei, thereby enabling the generation of transcriptomic and epigenomic profiles from as few as 10,000 cells²⁰. This enabled us to assess the transcriptomic and cis-regulatory element landscape of AgRP neurons during opposing states of energy availability as a means of identifying additional transcriptional pathways that underlie the

distinct cellular states exhibited by these neurons during periods of hunger and satiety.

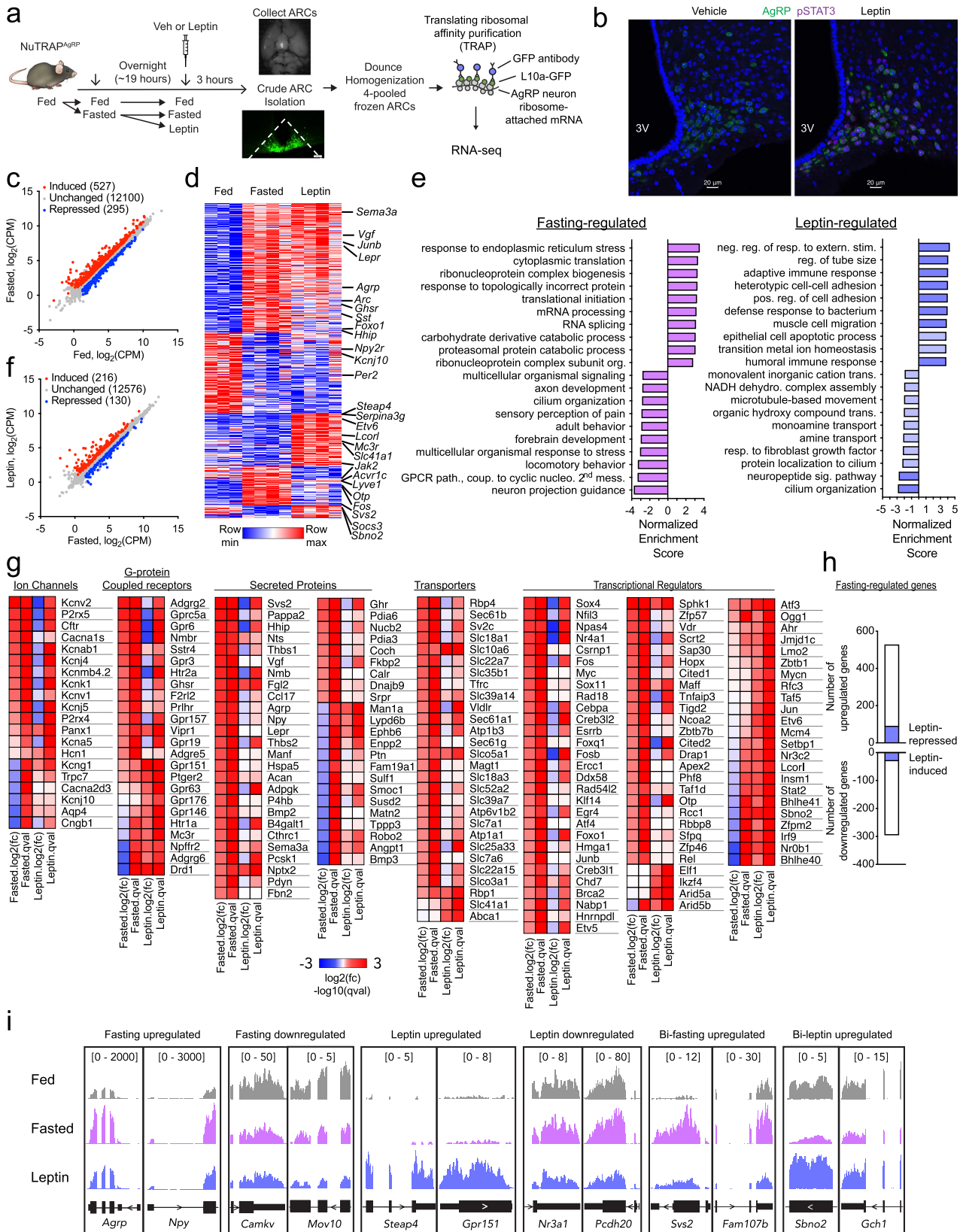
Results

Validating a transgenic tool for obtaining AgRP neuron-specific RNA-seq profiles

We previously developed a mouse model capable of providing cell type-specific transcriptional and epigenomic profiles from complex tissues, which we call NuTRAP (Nuclear tagging and Translating Ribosome Affinity Purification)²⁰. NuTRAP mice possess a loxP-stop-loxP sequence immediately upstream of a cassette that expresses a GFP-tagged L10a ribosomal subunit as well as mCherry-tagged RAN-GAP, which localizes to the nuclear membrane. Nuclei can be isolated by flow-sorting for either mCherry or GFP, as the GFP-tagged L10a ribosomal subunit is enriched in the nucleolus, thereby allowing for nuclear sorting. Crossing NuTRAP mice with either AgRP-IRES-Cre or POMC-IRES-Cre mice generates mice with tagged ribosomes or nuclei selectively within AgRP or POMC neurons of the ARC (here referred to as NuTRAP^{AgRP} or NuTRAP^{POMC}). Using this approach, tagged ribosomes can be isolated via affinity purification for RNA-seq, and tagged nuclei can be isolated via fluorescence-activated nuclear sorting (FANS) for ATAC-seq. We confirmed the viability of using NuTRAP^{AgRP} mice to generate cell-type specific transcriptional profiles by observing distinct gene expression patterns for GFP+ (AgRP neuron positive) and whole sample input ribosomes isolated from NuTRAP^{AgRP} mice using qPCR. Canonical AgRP neuron genes were enriched, including *AgRP* and *Npy*, whereas genes known to be de-enriched in AgRP neurons were found at reduced levels, such as *Pomc*, *Gfap*, *Mobp* (Fig. S1a). We also observed that TRAP performed on four pooled ARCs resulted in greater enrichment for AgRP neuron markers than that seen with a smaller number of ARCs (Fig. S1A). To overcome the observed minimal input requirements for, and the reliability of, TRAP we opted to use four pooled ARCs for the remainder of our TRAP studies. Next, RNA-seq was used to validate and extend our qPCR data. Again, as anticipated, the canonical marker genes *AgRP* and *Npy* were enriched in our AgRP neuronal population (Fig. S1b). We also observed enrichment for other genes known to be expressed in these neurons, including *Corin*, *Otp*, *Ghsr*, and *Acur1c* (Supplementary Data 1) (Henry et al., 2017). Notably, the *Serpina3* family of genes was markedly enriched in AgRP neurons, including *Serpina3c*, the third-most enriched transcript, along with *Serpina3i*, *Serpina3n*, *Serpina3g*, and *Serpina3h*, suggesting that this family might play an important role in the regulation AgRP neuron biology. *Lepr*, encoding the leptin receptor, was also significantly enriched in AgRP neurons. We then compared the transcriptomic profiles of NuTRAP^{AgRP} and NuTRAP^{POMC} GFP+ TRAP samples. POMC neuron marker genes *Pomc* and *Cartpt* were among the most POMC neuron-enriched genes, along with *Prdm12*, which is indispensable for the expression of *Pomc* (Fig. S1c)²¹. Based on these results we were confident that we could isolate and transcriptionally profile a purified population of AgRP neurons.

Obtaining AgRP neuron-specific transcriptional profiles in response to fasting and leptin

We next sought to assess transcriptional profiles of AgRP neurons during various states of energy balance using male NuTRAP^{AgRP} mice that were fed, fasted and leptin-treated ($n = 3-4$ samples per experimental condition, 4 pooled mouse ARCs per sample). Mice were either provided food *ad libitum* or were fasted overnight and then injected with either leptin (5 mg/kg i.p.) or vehicle; three hours later mice were sacrificed and the ARC dissected out for further study (Fig. 1a). The dose of leptin chosen was confirmed to activate leptin-signaling-mediated activation of STAT3 (assessed by phospho-STAT3) in the ARC, with substantial co-localization within the cell body of AgRP neurons (Fig. 1b). We identified 527 and 295 genes that were induced and repressed by fasting in AgRP neurons, respectively (Fig. 1c).



Among the fasting-induced genes were *AgRP*, *Npy*, and *Vgf*, all shown previously to be affected by food withdrawal (Campbell et al., 2017; Henry et al., 2015). Other genes exhibiting increased expression with fasting include *Acvr1c*, *Lys1*, *Svs2* (Fig. 1d, Supplementary Data 2). WebGestalt (WEB-based Gene Set Analysis Toolkit) gene set

enrichment analysis (GSEA) for gene ontology (GO) biological process revealed fasting-induced transcriptional programs that were associated with various molecular functions including, “response to endoplasmic reticulum stress” and “cytoplasmic translation”, and “ribonucleoprotein complex biogenesis”, among others (Fig. 1e).

Fig. 1 | Transcriptomic profiles of AgRP neurons during opposing states of energy balance. **a** Schematic of the experimental design. NuTRAP^{AgRP} mice were fed, then a subset were fasted overnight (-19 hr), following which mice were treated with IP vehicle or leptin (5 mg/kg). After 3 hours, mice were euthanized and ARCs were isolated, frozen, and homogenized according to the TRAP protocol. **b** Representative immunofluorescence image of ARC revealing induction of pSTAT3 45-minutes following leptin administration (right) compared to vehicle treatment (left); repeated independently 2 times. **c** Scatter plot showing comparing expression of genes within AgRP neurons from fasted versus fed littermates ($n = 4, 3$) [fold change >0.5 up (red) or down (blue), false discovery rate (FDR) < 0.05]; CPM, counts per million. The number of genes in a given expression profile is in parentheses. **d** Heatmap of differentially expressed genes in fed, fasted, and leptin-treated mice. **e** WebGestalt (WEB-based Gene Set ANalysis Toolkit) gene set enrichment analysis (GSEA) for geneontology biological process in either fasting-regulated (left, induced and repressed), or leptin-regulated (right, induced and repressed) transcriptional pattern categories with Normalized Enrichment Scores. All bars have an FDR < 0.05 except those that are light blue in the leptin-regulated

condition **f** Scatter plot showing regulated genes within AgRP neurons from leptin-treated versus fasted littermates ($n = 4, 4$) (fold change > 0.5 up (red) or down (blue), FDR < 0.05). CPM, counts per million. FDR-adjusted p-values with a threshold of 0.05 were generated using the Benjamini-Hochberg method to account for multiple comparisons. The number of genes in a given expression profile is in parentheses. **g** Heatmaps of selected gene categories. **h** Top: bar graphs showing the number of fasted up-regulated genes ($N = 527$) that are also down-regulated with leptin (blue bars, $N = 90$). Bottom: bar graphs showing the number of fasted down-regulated genes ($N = 295$) that are also up-regulated with leptin (blue bars, $N = 30$). **i** Genome browser views (in Integrative Genomics Viewer (IGV)) of RNA-seq tracks of representative fasting-upregulated, fasting-downregulated, leptin-upregulated, leptin-downregulated, bidirectional fasting upregulated (Bi-fasting upregulated), and bidirectional leptin upregulated (Bi-leptin upregulated) genes. The data from TRAP-seq experiments was generated from three independent biological replicates for fed mice, four independent biological replicates for fasted mice, and four independent biological replicates for leptin-treated mice.

These findings recapitulated our earlier work, and that of another group⁵¹. Within our dataset exist fasting-induced genes that are categorized as ion channels (e.g., *Kcnu2*, *P2rx5*, *Cftr*), G-protein coupled receptors (e.g., *Adgrg2*, *Gprc5a*, *Gpr6*), secreted proteins (e.g., *Agrp*, *Sus2*, *Vgf*), transporters (e.g., *Rbp4*, *Sec61b*, *Sc2c*), and transcriptional regulators (e.g., *Sox4*, *Nfil3*, and *Npas4*; Fig. 1g). Unsurprisingly, many transcripts encoding classic immediate early genes (IEGs) were upregulated in AgRP neurons during fasting (e.g., *Nr4a1*, *Fos*, *Myc*, *Fosb*, *Egr1*, *Junb*), potentially driven by the sustained increase in neuronal firing that occurs throughout the course of food deprivation²².

In leptin-treated mice, we observed the induction of 216, and repression of 130, genes in AgRP neurons (Fig. 1f). *Socs3*, a component of the leptin signaling negative feedback loop, was significantly upregulated in response to leptin-treatment. Notably, leptin-induced transcriptional programs were associated with biological processes including “negative regulation of response to external stimulus”, “regulation of tube size”, and “adaptive immune response”, among others (Fig. 1e). Leptin-induced genes included those encoding ion channels (e.g., *Trpv6*, *Kcng1*), G-protein coupled receptors (e.g., *Drd1*, *Adgrg6*, *Gpr151*), secreted proteins (e.g., *Man1a*, *Lypd6b*, *Ephb6*), transporters (e.g., *Rbp4*, *Slc41a1*, *Abca1*), and transcriptional regulators (e.g., *Stat2*, *Bhlhe41*, and *Sbno2*) (Fig. 1g).

We were particularly interested in identifying “bidirectional” transcriptional changes in response to fasting and leptin (i.e., genes induced by fasting and repressed by leptin, or vice versa). This analysis revealed 120 genes exhibiting a bidirectional expression pattern, including 90 genes induced by fasting and repressed by leptin (e.g., *Acr1c*, *Gpr157*, *Lyve1*, and *Otp*), and 30 repressed by fasting and induced in response to leptin (e.g., *Sbno2*, *Serpina3i*, *Drd1*, *Man2a1*) (Figs. 1h, 1i). Expression of this set of 30 genes is reduced in response to fasting, a state that has classically been associated with a marked decline in serum leptin levels and leptin signaling, while their expression is increased in response to the administration of exogenous leptin in the fasted state²³. Given the apparent bi-directional leptin sensitivity of these 30 genes, it is conceivable that leptin depletion-driven declines in the expression of these genes may mediate the adaptive physiological response to starvation attributed to the loss of leptin in the fasted state²³. We also performed TRAP-seq on fed, fasted and leptin-treated NuTRAP^{Pomc} samples and observed relatively few significantly changed genes in response to fasting, a finding that recapitulated earlier work, and prompted us to focus on AgRP neurons for the remainder of our studies (Fig. S1d)⁵.

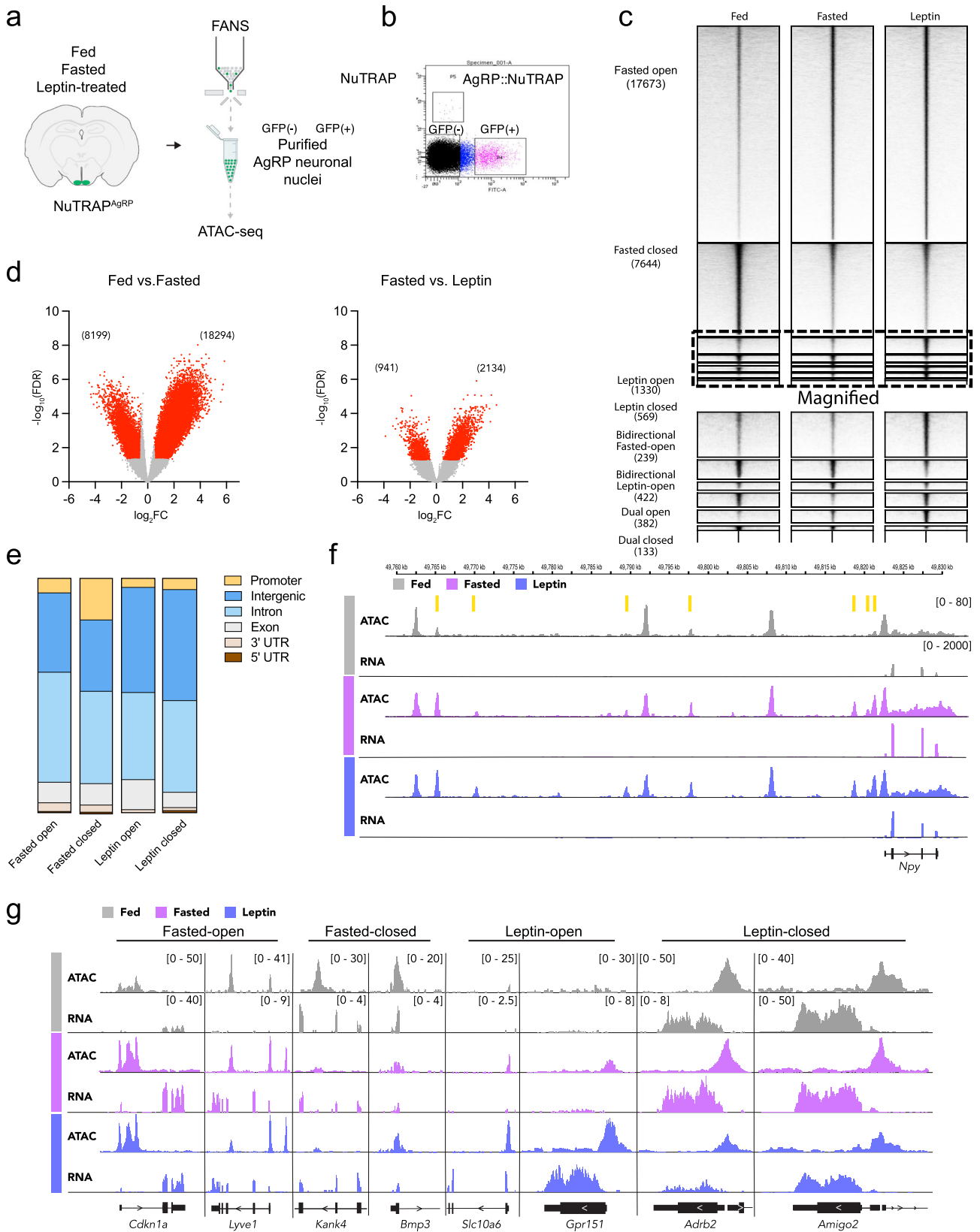
Validating a transgenic tool for obtaining AgRP neuron-specific ATAC-seq profiles

Next, we confirmed the feasibility of using NuTRAP mice to assess chromatin state in AgRP neurons. Using pooled male NuTRAP^{AgRP}

mouse ARCs, we isolated and sorted 10,000 nuclei, and then performed Assay for Transposase Accessible Chromatin with high-throughput sequencing (ATAC-seq) for AgRP positive (GFP+) and negative (GFP-) populations from the same pooled samples (Fig. 2a, b). We detected 15,530 and 9029 closed chromatin regions that are specifically enriched in AgRP positive neurons (Fig. S2a), and principal components analysis (PCA) showed a clear distinction between the two populations in terms of their respective chromatin states (Fig. S2b). We next examined the chromatin state of AgRP neurons at key genes expressed in AgRP neurons, compared to that of the non-AgRP neuron population, and observed that AgRP neurons exhibited a selective enrichment of open chromatin regions (OCRs) at the promoters and enhancers of *Agrp*, *Npy*, and *Corin*, among others (Fig. S2c). We also observed multiple OCRs upstream of *Lepr* in AgRP neurons (Fig. S2d). Interestingly, these *Lepr*-associated OCRs are distinct from those observed in hepatocytes, suggesting that putative enhancer elements for *Lepr* may be developmentally divergent. We also detected OCR de-enrichment at the promoter of *Slc17a6*, which encodes the protein vesicular glutamate transporter 2 (VGlut2), reflecting the fact that AgRP neurons are gabaergic, rather than glutamatergic (Fig. S2c). Moreover, de-enrichment of OCRs was noted at non-neuronal marker genes, such as those for oligodendrocytes (e.g., *Olig1* and *Olig2*) and tanycytes (e.g., *Sox2*), supporting the utility and fidelity of our method for obtaining low-input AgRP neuron-specific ATAC-seq profiles (Fig. S2c).

AgRP neuron-specific ATAC-seq profiles in response to fasting and leptin

We next performed ATAC-seq on AgRP neurons from fed, fasted, and leptin-treated male NuTRAP^{AgRP} mice. Of the 90,196 called ATAC-seq peaks in our dataset, we detected 18,294 fasted-opened and 8189 fasted-closed regions, and 2134 leptin-opened and 941 leptin-closed regions of chromatin (Fig. 2c, d). We also detected changes in chromatin accessibility that were bidirectional (i.e., reciprocally regulated in fasted vs. leptin-treated) or dually enriched (i.e., open in response to both fasting and leptin-treatment) (Fig. 2c). The majority of differentially expressed ATAC peaks were found within intergenic (36–45%) and intronic (43–50%) regions, while only 3–11% of ATAC-peaks were found within gene promoter regions, defined as regions <1000 bps upstream of the transcriptional start site (TSS) (Fig. 2e), a changed genomic distribution of changed chromatin accessibility previously exhibited by activated neurons (Su et al., 2017). We observed areas of chromatin that became more accessible with fasting (i.e., fasted-opened) near various genes known to be enriched in response to fasting in AgRP neurons, including *Npy* (Fig. 2f, g). Moreover, we also observed areas of chromatin that became less accessible with fasting (i.e., fasted-closed), as well as those that became more or less accessible with leptin (i.e., leptin-opened and leptin-closed) (Fig. 2g).



Uncovering transcriptional regulators that control AgRP neuron biology

Having generated an extensive atlas of dynamic chromatin regions in AgRP neurons in response to fasting and leptin treatment, we next sought to determine which TFs might bind to these regions. To accomplish this we performed Analysis of Motif Enrichment (AME), a

program of the MEME suite, on chromatin regions with a high likelihood of impacting fasting- and leptin-induced transcriptional changes (Fig. 3a)²⁴. To accomplish this, we filtered ATAC-seq peaks to retain those within ± 200 kb of a TSS corresponding to a gene whose expression is concordantly regulated (e.g., fasting-induced, gained-open ATAC-seq peaks near fasting-induced genes; hereafter called

Fig. 2 | Alterations in energy availability impact the chromatin landscape of AgRP neurons. **a** Experimental schematic. ARCs from fed, fasted, and leptin-treated NuTRAP^{AgRP} mice were isolated followed by nuclear isolation. 10,648 ± 1489 nuclei, from 4 mice, were pooled for each condition (fed, fasted, leptin-treated) before being subjected to ATAC-seq. **b** FACS plot of single nuclei with FITC (GFP) fluorescence on the x-axis and mCherry fluorescence on the y-axis, with filtering gates showing discrete populations for NuTRAP^{AgRP} GFP⁺ and GFP⁻ nuclei. **c** Heatmap showing differentially expressed OCRs for each of the treatment conditions clustered into one of eight patterns (rows). Amplitude of each peak center (±5 kb) is represented in black as indicated. **d** Volcano plots showing differentially expressed OCRs in fasted vs. fed mice (left, $n = 2, 2$) or leptin vs. fasted mice (right, $n = 2, 2$). Red dots correspond to significantly different gained-open and gained-

closed regions [fold change >0.5 up (red) or down (red), FDR < 0.05]; CPM, counts per million. Peaks with a CPM < 1 were not included in volcano plot. FDR-adjusted p-values with a threshold of 0.05 were generated using the Benjamini-Hochberg method to account for multiple comparisons. **e** Bar graphs revealing the genomic features of fasted-opened, fasted-closed, leptin-opened, leptin-closed ATAC-seq peaks. **f** Genome browser views (IGV) of ATAC-seq peaks within the vicinity of the *Npy* gene. Yellow bars correspond to fasted-opened ATAC-peaks. **g** Genome browser views (IGV) of representative Fasted-opened, Fasted-closed, Leptin-opened, and Leptin-closed ATAC-seq peaks near the indicated genes. The data from ATAC-seq experiments was generated from two independent biological replicates for fed mice, two independent biological replicates for fasted mice, and two independent biological replicates for leptin-treated mice.

concordant fasted-opened; Fig. 3a, S3a). We observed that 96% ($p = 1.39 \times 10^{-9}$), 78% ($p = 1.17 \times 10^{-8}$), 59% (N.S.), and 51% (N.S.) of fasting-induced, fasting-repressed, leptin-induced, and leptin-repressed genes, respectively, were associated with a concordant peak (Fig. S3b). Thus, up-regulated genes were significantly more likely to be close to an up-regulated peak in the same condition, but this was not true for down-regulated genes. The majority of genes associated with a concordant peak were in fact associated with numerous concordant peaks; most genes were associated with 4–6 peaks for fasting-induced genes, and 1–3 peaks per genes for the other three comparisons (Fig. S3c). We also observed a positive relationship between the number of concordant peaks and the fold-change of the associated gene (Fig. S3d). The number of concordant peaks identified for each of the four comparisons was 2452 fasted-opened, 531 fasted-closed, 203 leptin-opened, and 74 leptin-closed (Fig. 3b).

We next performed motif enrichment analysis on the four distinct sets of concordant peaks (i.e., fasted-opened, fasted-closed, leptin-opened, leptin-closed), while employing 6 different background control peak sets. Thus, in all, 6 separate instances of AME were performed for each peak set. Motifs were considered further only if they were enriched in ≥5 out of 6 AME instances (Fig. S3a, S3e, S3f). We observed that motifs associated with the AP-1 transcription factor family were highly enriched in concordant fasted-opened peaks, including motifs for FOSB, JUNB, ATF3, JUN, and JUND (Fig. 3c, d). This finding was unsurprising given that these activity-dependent TFs have been implicated as being permissive for the physiological changes that enable neurons to increase their firing rate²⁵. Reassuringly, STAT3 was the most enriched TF motif in leptin-opened peaks, consistent with its established role as a key mediator of leptin-induced transcriptional regulation (Fig. 3c).

We next set out to develop a prioritized list of TFs that might drive the expression of genes that increase AgRP neuron firing during fasting. We reasoned that such TF motifs would be enriched in concordant fasted-opened and leptin-closed peaks, but not in concordant leptin-opened or fasted-closed peaks. With this approach, we identified 101 TF motifs that were enriched in concordant fasted-opened and leptin-closed peaks (Fig. 3e). Of these motifs, only 4 were not also enriched in concordant leptin-opened and fasted-closed peaks (Fig. 3f). Upon ranking these motifs by their summed motif score, PRGR and ANDR, two transcription factors not previously implicated in the control of AgRP neuron biology, were the most enriched (Fig. 3g). We also identified 14 TF motifs that were exclusively enriched in fasted-opened peaks, with the MAF transcriptional factor family members, MAFB, MAFK and MAFG having been particularly enriched (Figs. 3d, 3h).

Next, we developed a prioritized list of TFs that potentially drive the expression of genes that decrease AgRP neuron firing after leptin treatment. We reasoned that such associated TF motifs would be enriched in the two distinct sets of concordant leptin-opened peaks and fasted-closed peaks, but not fasted-opened or leptin-closed peaks. We identified 127 TF motifs that were enriched in both concordant leptin-opened and fasted-closed peaks (Fig. 3i). Of these, 16 TF motifs were also not enriched in fasted-opened or leptin-closed peaks

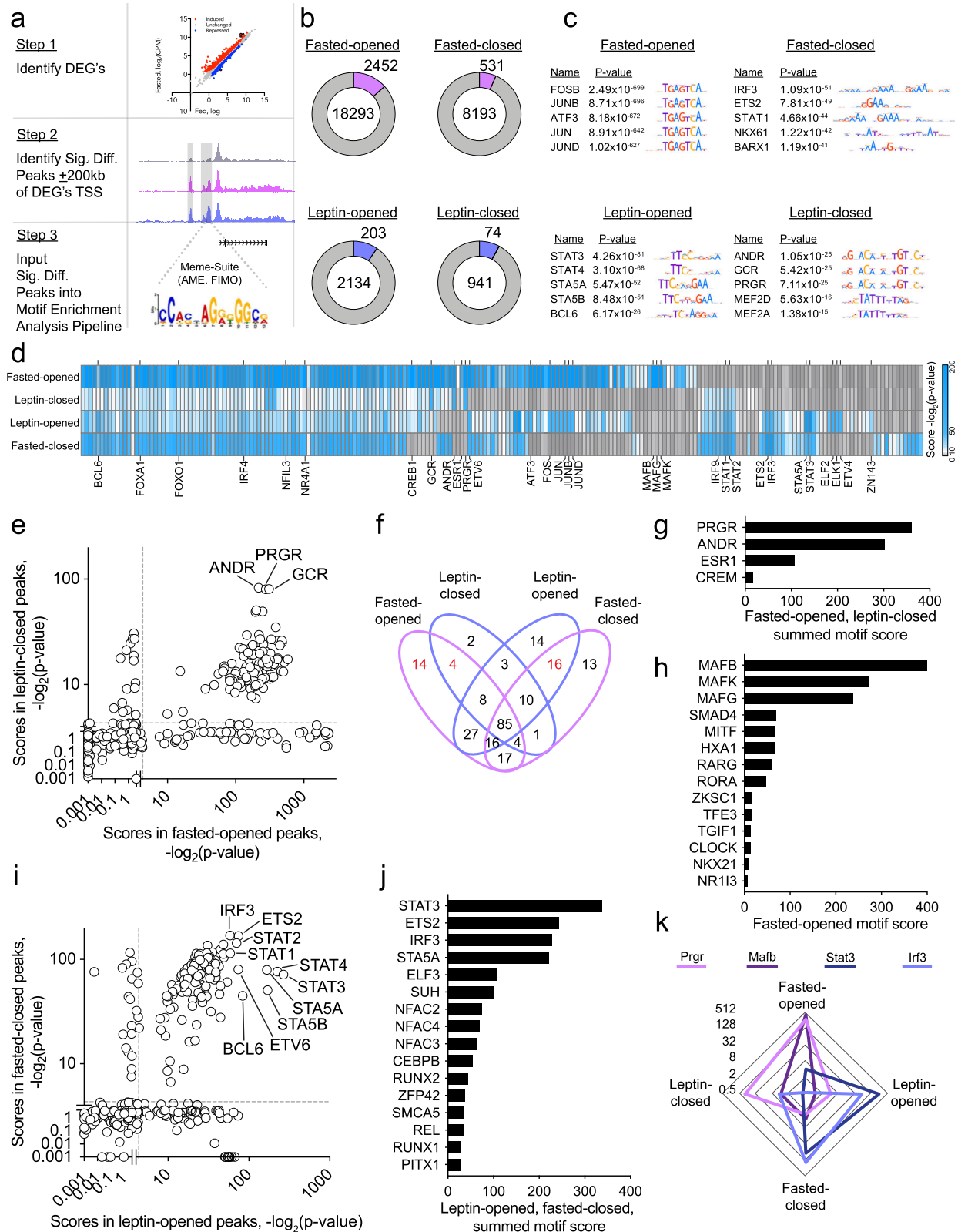
(Fig. 3f). We then ranked these 16 TF motifs based on their summed motif scores (summed motif enrichment scores in leptin-opened and fasted-closed peaks) (Fig. 3j). With this approach we found several motifs that corresponded to TFs that have not been linked to the neural control of energy homeostasis, including interferon regulatory factor 3 (IRF3), which had the most significant concordant fasted-closed motif enrichment score, and third most significant summed motif score, behind only STAT3 and ETS2 (Fig. 3i). Moreover, the IRF3 motif enrichment profile was similar to that of STAT3, and distinct from those enriched in fasted-open and leptin-closed areas of chromatin (e.g., PRGR, MAFB) (Fig. 3k).

Leptin activates neuronal IRF3

Irf3 mRNA is expressed in AgRP neurons; we saw no change in *Irf3* levels with fasting or leptin treatment (Fig. 4a), which was unsurprising given that *Irf3* is not nutritionally regulated in other cell types^{26,27}. We also noted the existence of an OCR near the *Irf3* TSS (Fig. 4a). Additionally, we detected IRF3 protein expression within the ARC of adult male mice using immunofluorescence (Fig. 4b).

In immune cells, adipocytes, and other cells, IRF3 is a key component of the antiviral innate immune system and can be activated by three established pathways: (1) dsRNA → Tlr3/4; (2) dsRNA → MDA5/Rig-1; or (3) dsDNA → cGAS. Upon activation by upstream kinases, IRF3 translocates from the cytosol into the nucleus to activate gene expression²⁸. Interestingly, in contrast to other toll-like receptors, Tlr3 was appreciably detected in AgRP neurons, suggesting a potential role for Tlr3 → Irf3 activation in AgRP neurons (Fig. S4a). Moreover, in addition to Tlr3 and its signaling components, the MDA5/Rig1 pathway is also expressed, all of which suggest a potential route and role for IRF3 activation in AgRP neurons (Fig. S4b, c). Interestingly, many canonical inflammatory genes (e.g., *Isg15*, *Rsad2*, *Oasl1*, *Ccl5*) which have been linked to IRF3 activation in macrophages, hepatocytes, and other cell types are very lowly, if at all, expressed, in AgRP neurons, either in the presence or absence of leptin. Using ATAC-seq data from hepatocytes as a comparator, we note that various known IRF3 target genes that are expressed in hepatocytes but not in AgRP neurons (e.g., *Rsad2*, *Isg15*, *Ccl5*, and *Oasl2*) are associated with OCRs in hepatocytes only (Fig. S4d). Thus, we predict that the transcriptional targets of IRF3 in AgRP neurons are distinct from those found in other cell-types.

To determine if IRF3 is activated by leptin, we employed an *in vitro* model. GT1-7 cells are an immortalized mouse gonadotrophin-releasing hormone (GnRH)-expressing hypothalamic neuronal cell line that are rendered leptin responsive when transfected with the leptin receptor²⁹; the leptin-responsivity of these cells was confirmed by detecting an increase in pSTAT3 following leptin-treatment (Fig. 4c, S4e). GT1-7 cells were co-transfected with plasmids expressing the long-form of the mouse leptin receptor, and IRF3-GFP, respectively. These cells were then treated with either vehicle or 100 nM leptin prior to being subjected to live cell imaging. With this approach we observed a pronounced induction in nuclear translocation of IRF3 upon treatment with leptin at the 5-hour time point (Fig. 4b). A similar time course of IRF3 activation has been demonstrated using models of



Poly(I:C)-driven IRF3 action HT-29 cells³⁰. These results are consistent with a model whereby leptin induces the activation of neuronal IRF3 in a cell-autonomous manner.

To determine whether leptin activates IRF3 in vivo, whole hypothalamus was collected from wild-type male C57BL6/J mice 5 h after treatment with either vehicle or leptin, an approach we confirmed is

suitable for detecting leptin-induced nuclear pSTAT3 (Fig. S4f). Isolated nuclei were treated with an IRF3 antibody and fluorescent secondary antibody and subjected to flow cytometry (Fig. 4e). With this approach we detected a significant increase in nuclear IRF3 following leptin-treatment, a finding that demonstrates the ability of leptin to activate IRF3 within the mouse hypothalamus (Fig. 4f).

Fig. 3 | Integrated transcriptomic and cistromic analysis identifies putative leptin-sensitive TFs in AgRP neurons. **a** Schematic showing the broad computational heuristic employed to identify putative pro-satiety TF motifs. Step 1: Identify fasted-induced, fasting-repressed, leptin-induced, and leptin-repressed differentially expressed genes (DEGs). Step 2: Determine significantly different fasted-opened, fasted-closed, leptin-opened, and leptin-closed ATAC-seq peaks, and identify those that are ± 200 kb upstream and downstream of those DEGs identified in Step 1 (e.g., concordant leptin-opened peaks). Step 3: Perform motif enrichment analysis on the peaks identified in Step 2. **b** Pie charts showing the total number of peaks classified as fasted-opened, fasted-closed, leptin-opened or leptin-closed, as well as the subset of concordant peaks (lavender and blue bars). For this analysis, we filtered non-chromosomal features (scaffolds); there were 8 such instances in the fasted vs fed comparison and none in the leptin vs. fasted comparison. **c** TF motifs enriched in concordant fasted-opened, fasted-closed, leptin-opened and leptin-closed ATAC-seq peaks. **d** Heatmap showing motif scores [$-\log_2(p\text{-value})$]

concordant fasted-opened, leptin-closed, leptin-opened, and fasted-closed ATAC-seq peak sets. **e** Comparison of TF motif enrichment scores for fasted-opened peaks vs. leptin-closed peaks. **f** Venn diagrams showing the number of TF motifs enriched in concordant fasted-opened, leptin-closed, leptin-opened, and/or fasted-closed ATAC-seq peaks. **g** Summed motif enrichment scores from fasted-opened and leptin-closed TF motifs. **h** Motif enrichment scores from fasted-opened TF motifs. **i** Comparison of TF motif enrichment scores for leptin-opened peaks vs. fasted-closed peaks. **j** Summed motif enrichment scores from leptin-opened and fasted-closed TF motifs. **k** Radar plot showing the TF motif enrichment scores ($-\log_2(p\text{-value})$) with 4 axis with a \log_2 scale, all for concordant fasted-opened, leptin-closed, leptin-opened, and fasted-closed ATAC-seq peak sets. Profiles shown are for PRGR, MAFB, STAT3, and IRF3. For AME analysis, the term p-value is the optimal enrichment p-value of the motif according to the statistical test, adjusted for multiple tests using a Bonferroni correction.

IRF3 mediates leptin-induced satiety in AgRP neurons

We have previously observed that whole body IRF3 knockout mice are hyperphagic on a high-fat diet compared to control mice, a finding that was at the time interpreted as a compensatory mechanism to offset the increased energy expenditure that these mice exhibit²⁷. Here we asked whether IRF3 mediates the hunger-suppressive effects of leptin directly. We generated male AgRP-ires-Cre::Irf3^{fl/fl} (AgI3KO) mice as a means of deleting IRF3 selectively within AgRP neurons. No change in chow-fed body weight or cumulative food intake was apparent during basal conditions in AgI3KO mice (Fig. S5a, b). We next implemented an established fasting-refeeding paradigm to assess leptin-induced satiety (Fig. 5a). In this paradigm, leptin-treated AgI3KO mice exhibited greater 24-hour cumulative food intake upon refeeding than control mice, indicating blunted sensitivity to leptin (Fig. 5c). Of note, control mice reduced their food consumption by 1.14 gm over 24 hours, while AgI3KO mice reduced their intake by only 0.38 gm over the same time period, a 67% reduction in leptin action. The reduced responsiveness to leptin exhibited by AgI3KO mice is unlikely to be due to general hyperphagia, or greater sensitivity to starvation, per se, as no difference was observed between vehicle-treated fasted-refed AgI3KO mice and control mice (Fig. 5b).

IRF3 is activated by viral RNA binding to Toll-like receptor 3 (TLR3), which is enriched in AgRP neurons relative to other TLRs (Fig. S4a). The synthetic (TLR3) ligand polyinosinic:polycytidylic acid (poly(I:C)), a known activator of IRF3, induces reduced locomotion, anorexia, and early phase hyperthermia followed by a late phase (8–16 hours) hypothermia^{31,32}. Interestingly, leptin has been shown to produce not only anorexia, but also an alteration in core body temperature that resembles a sickness response³³. Thus, given the high probability that AgRP neurons are a component of the neural ensemble involved in the sickness response, we asked whether IRF3^{AgRP} may mediate behavioral and physiologic responses to leptin that are commonly observed during a sickness response (i.e., reduced locomotion and derangements in thermoregulation). To this end, telemetry probes were implanted in AgI3KO and control mice to measure core body temperature and locomotor activity (LMA) in two-dimensional space, and vehicle or leptin was infused directly into the ARC (Fig. 5d). Leptin-treated control mice exhibited a decrease in late-phase (8–16 hours) core body temperature (* $P = .0402$) (Fig. 5e, f). Leptin-treated AgI3KO mice exhibited a late-phase (8–16 hour) core body temperature that was significantly higher than that of control mice (Fig. 5e, h, S5c), despite no difference in core body temperature between vehicle-treated control and AgI3KO mice (Fig. 5e, g, S5c). Moreover, leptin significantly reduced LMA in control mice (* $P = .0172$), while there was a trend ($p = 0.07$) towards increased LMA in AgI3KO mice after leptin (Fig. S5d–f). Thus, these findings demonstrate the blunted effects of leptin on mice devoid of IRF3 in AgRP neurons.

To assess whether IRF3 activation in AgRP neurons is sufficient to suppress food intake, we utilized a gain-of-function mouse model in

which Ser388/Ser390 of IRF3 are mutated to phospho-mimetic Asp residues (S \rightarrow D), creating a constitutively active allele that is expressed in a Cre-dependent manner (the allele and mouse are hereafter referred to as IRF3-2D)³⁴. These IRF3-2D mice were crossed to AgRP-IRES-Cre mice, thereby generating AgIRF3-2D mice which expressed the constitutively active version of IRF3 in their AgRP neurons (Fig. S5f). In vivo flow cytometry analysis revealed an increase in nuclear IRF3 within hypothalamic nuclei of AgI3-2D mice (Fig. S5g). As predicted, fasted, vehicle-treated, male AgI3-2D mice have suppressed food intake following a period of fasting, thus mimicking that of control mice treated with leptin (Fig. 5g, h).

Discussion

While the ability of leptin to evoke prolonged changes in food consumption has largely been attributed to its engagement of the transcriptional effector STAT3, we lack a complete roster of leptin-sensitive TFs in any cell type³. Converging findings indicate a role for leptin-sensitive, STAT3-independent transcriptional effectors. For instance, the dose of leptin required to suppress food intake in rats is much higher than the dose required to produce maximal STAT3 activation (i.e., phospho-STAT3) within the ARC, suggesting that leptin-mediated activation of pSTAT3 is not sufficient to yield a full satiety-evoking effect³⁵. Moreover, mice lacking STAT3, or the tyrosine residue of LepR that recruits STAT3 (Tyr₁₁₃₈), are less obese than mice lacking either leptin (*ob/ob*) or the leptin receptor (*db/db*), and leptin signaling remains partially intact in these mice³⁶. These results suggest the existence of a STAT3-independent arm of LepR signaling. Interestingly, LepRb sequences between residues 921 and 960 have been implicated as indispensable for the STAT3-independent component of leptin's metabolic actions³⁶. Our data indicates a role for IRF3 as a transcriptional mediator of leptin action in AgRP neurons.

Our simultaneous examination of transcriptomic and chromatin accessibility landscapes during opposing states of hunger and leptin-induced hunger-suppression enabled us to generate a list of candidate TFs that potentially regulate hunger in a leptin-dependent manner. The observation that the IRF3 motif was enriched in concordant leptin-opened peaks suggested that leptin-driven activation of IRF3 may be permissive for the expression of “hunger-suppressing” transcriptional programs in AgRP neurons. Consistent with this model, loss-of-function AgI3KO mice exhibited reduced leptin-induced suppression of hunger during a fasting-refeeding paradigm. Alternatively, or in addition, the finding that the IRF3 motif was enriched in concordant fasted-closed peaks suggested that the loss of IRF3 activity might be permissive for expression of “pro-hunger” transcriptional programs in AgRP neurons in the fasted state. Given the decline in serum leptin levels and leptin signaling during the fasted state, it stands to reason that a decline in IRF3 activity during fasting might be necessary for the establishment of a “pro-hunger” transcriptional state in AgRP neurons. Consistent with this model, gain-of-function AgI3-2D mice exhibited

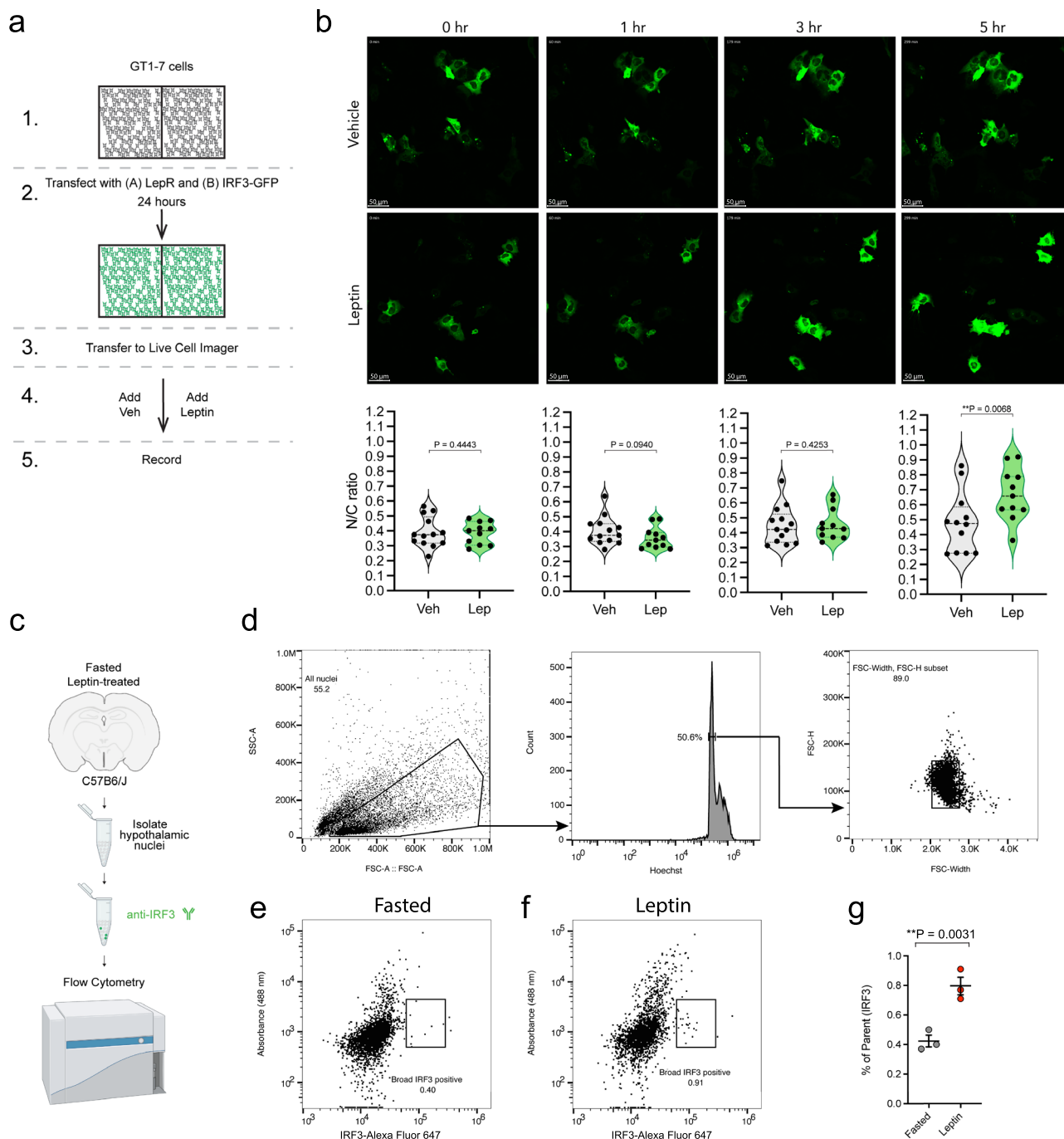
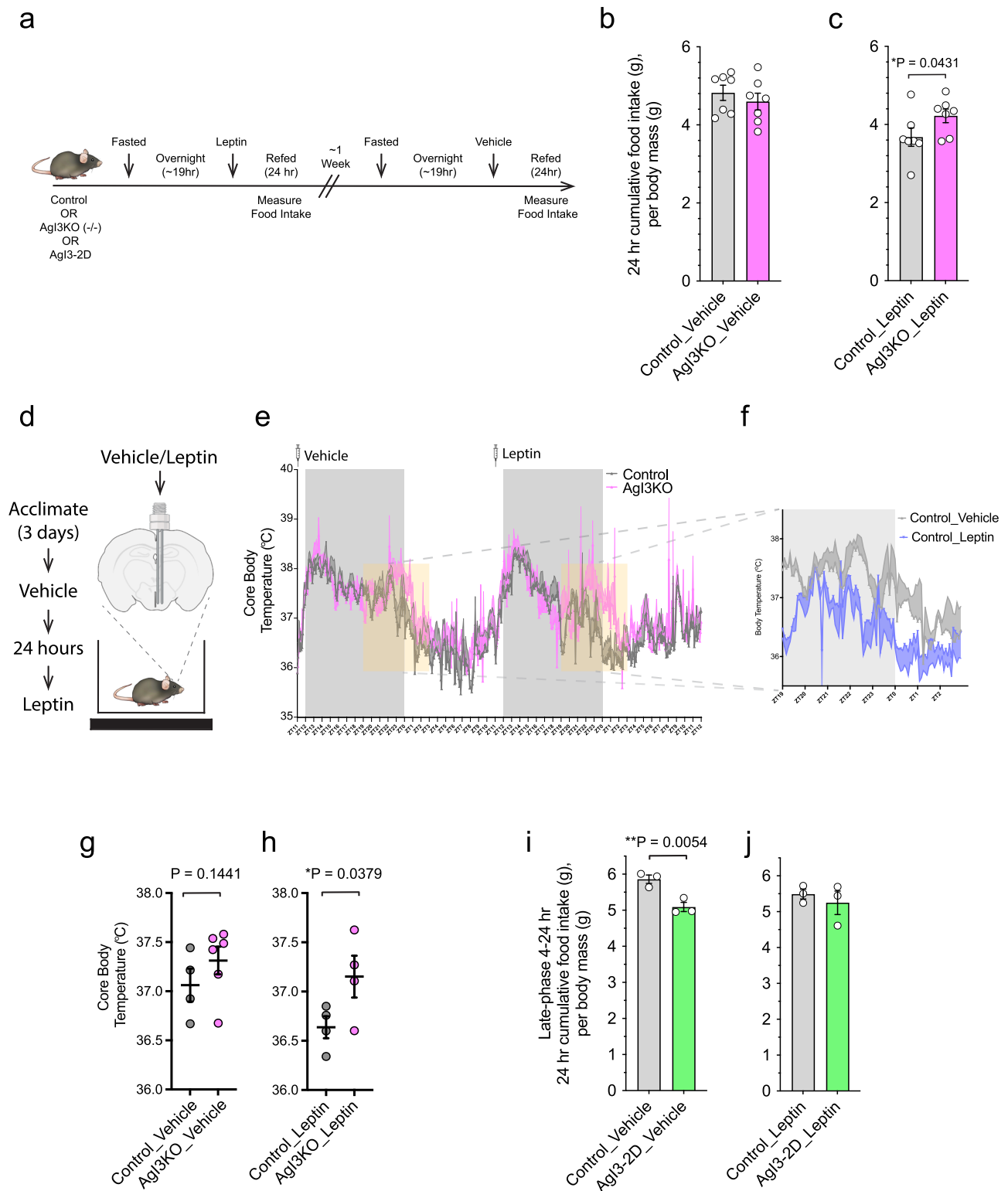


Fig. 4 | Leptin activates IRF3 in a cell autonomous manner. a Schematic of in vitro GT1-7 live-cell imaging experiment. **b** Representative images showing the dynamic imaging of GFP-tagged IRF3 in response to vehicle or leptin stimulation in GT1-7 cells expressing both IRF3-GFP and leptin receptor at 0, 1, 3, and 5 hours after stimulation. Quantification of nuclear/cytoplasmic (N/C) GFP signal is shown at each time point. Each dot represents a single tracked cell ($n = 13$, II). At $T = 5$ hours ($p = 0.0068$, $t = 2.681$, $df = 22$). The violin plots indicate median values (wide dashed middle line), first and third quartiles (narrow dashed lines); this finding recapitulated an earlier observation from a pilot experiment. **c** Schematic of in vivo IRF3 flow cytometry experiment. **d** Flow cytometry gating strategy. Particles smaller than nuclei (black dots) were eliminated with an area plot of forward-scatter (FSC-A) versus side-scatter (SSC-A), with gating for nuclei-sized particles

inside the gate (box)⁵². 2 N Hoechst 33342 stained nuclei were positively gated to avoid nuclei doublets. Plots of width versus height, both in the forward-scatter channel were used to further exclude aggregates of two or more nuclei. **e, f** Two representative scatter plots of IRF3-Alexa Fluor 647 primary and secondary staining (x-axis) and empty 488 channel (y-axis) were used to identify the IRF3-positive population for the fasted (**e**) and leptin-treated (**f**) conditions. **g** Results of the fasted and leptin % of Parent IRF3 signal comparison. Results are presented as mean values \pm SEM and analyzed by a one-tailed student t-test ($p = 0.0031$, $t = 5.251$, $df = 4$). This finding was replicated once. The flow cytometry results were generated from three independent biological replicates for fasted mice, and three independent biological replicates for leptin-treated mice.



reduced hunger when tested in the fasting-refeeding paradigm. Given these findings, we propose that IRF3 represents a leptin-sensitive TF that bidirectionally regulates hunger, with the loss of leptin-mediated IRF3 signaling in the fasted state representing a critical “pro-hunger” event, and the resurgence in leptin-mediated IRF3 signaling in the leptin-treated state representing a key “hunger-suppressing” event. IRF3 has been chiefly studied as a core component of the innate immune antiviral response pathway, with viral pathogen-associated molecular patterns (PAMPs) binding to TLR3/4 and activating the

cGAS-STING/TBK1 pathway, resulting in phosphorylation and nuclear translocation of IRF3^{37,38}. The signal transduction mechanisms linking leptin receptor to IRF3 remain to be determined, but we note that several of the known upstream activators of IRF3 (e.g., cGAS, STING, and IKKε) are not expressed in AgRP neurons, according to our RNA-seq results. It is interesting to speculate that PI3K-Akt, a known but poorly understood arm of the leptin signaling pathway, may be involved. This hypothesis is supported by data showing that macrophage IRF3 is phosphorylated and activated by Akt, and this activation

Fig. 5 | IRF3 in AgRP neurons mediates leptin-induced behavioral alterations. **a** Schematic of fasting-refeeding experimental paradigm. Control and AgI3KO mice were fasted overnight, followed by refeeding in the presence of leptin; food intake was measured over a 24-hour period. After a week, the same mice were subjected to the same paradigm, except vehicle was administered instead of leptin. **b** 24-hour cumulative body-weight adjusted food intake measured in fasted-refed, vehicle-treated, control and AgI3KO mice ($n = 7, 7$). **c** 24-hour cumulative body-weight adjusted food intake measured in fasted-refed, leptin-treated, control and AgI3KO mice ($n = 7, 7$). Results are presented as mean values \pm SEM and analyzed by a one-tailed student t-test ($p = 0.0431$, $t = 1.869$, $df = 12$). Food intake study data (Fig. 5b, c) were generated from seven independent biological replicates for control mice, and seven independent biological replicates for AgI3KO mice. Each circle denotes a single mouse. Results are mean \pm SEM of each condition and analyzed by a one-tailed student t-test. **d** Schematic showing the time-course and experimental paradigm of vehicle- and leptin-treatment telemetry experiments. **e** Core body temperature measures during a 48-hour period showing control mice that received vehicle and leptin-treatment (5 mg/kg) in control mice or AgI3KO mice ($n = 4, 6, 4, 4$). The syringes and transparent yellow boxes illustrate the times of vehicle/leptin injection and the 8-hour epochs used for analyzes, respectively. **f** Inset image showing superimposed Control_Vehicle and Control_Leptin core body temperature

plots during their respective second 8-hour recording epochs. **g** Average core body temperature following vehicle-treatment for control and AgI3KO mice, with each mouse's mean value during the 8-hour period depicted ($n = 6, 3$). **h** Average core body temperature following leptin-treatment for control and AgI3KO mice, with each mouse's mean value during the 8-hour period depicted ($n = 3, 3$). Core body temperature study data in Fig. 5G were generated from four independent biological replicates for control mice, and six independent biological replicates for AgI3KO mice. Results are presented as mean values \pm SEM and analyzed by a one-tailed student t-test ($p = 0.1441$, $t = 1.138$, $df = 8$). Core body temperature study data in Fig. 5H were generated from four independent biological replicates for control mice, and four independent biological replicates for AgI3KO mice. Results are presented as mean values \pm SEM and analyzed by a one-tailed student t-test ($p = 0.0379$, $t = 2.143$, $df = 6$) **i** 4-24-hour body weight adjusted cumulative food intake measured by fasted-refed, vehicle-treated, control and AgI3KO mice ($n = 3, 3$). Results are presented as mean values \pm SEM and analyzed by a one-tailed student t-test ($p = 0.0054$, $t = 4.507$, $df = 4$) **j** 4-24-hour body weight adjusted cumulative food intake measured by fasted-refed, leptin-treated, control and AgI3KO mice ($n = 3, 3$). Food intake study data (Figs. 5i, 5j) were generated from three independent biological replicates for control mice, and three independent biological replicates for AgI3KO mice. Each circle denotes a single mouse.

is blocked by the PI3K inhibitor wortmannin^{39,40}. Future studies will address potential leptin \rightarrow PI3K/Akt \rightarrow IRF3 pathway and its contribution to leptin-induced satiety.

Mice with IRF3 ablation in AgRP neurons exhibited blunting of leptin sensitivity, yet did not exhibit either a basal or high-fat diet-induced increase in body weight. This finding is not unexpected. First, Cre-loxP deletion of *Lepr* from AgRP neurons results in only a mild increase in body mass and composition that was primarily driven by decreased energy expenditure, as no change in basal food intake was detected⁴¹. More recently, CRISPR-Cas9-mediated genetic ablation of *Lepr* in AgRP neurons of adult mice was shown to cause an increased body weight phenotype that recapitulated that observed with whole-body *Lepr* null mice, suggesting that deletion of the leptin receptor early in development results in yet-to-be elucidated compensation that preserves the function of the core homeostatic regulatory machinery⁴. A similar developmental compensation may contribute to the lack of a body weight phenotype in our AgI3KO mice. There is known functional redundancy between IRF3 and IRF7, and IRF7 or another TF (e.g., STAT3, STAT1), may be able to compensate for the absence of IRF3³⁷. It should be mentioned that there is precedent for Cre-loxP deletion of a suspected “pro-satiety” transcription factor abrogating leptin-induced satiety in the absence of a body weight phenotype, as was observed with the deletion of ATF3 from leptin receptor-expressing cells (Allison et al., 2018). Future studies should assess the impact of loss of IRF3 in adult AgRP neurons using a time-restricted approach. Moreover, our study was designed to identify transcriptional regulators that influence AgRP neuronal biology after an acute administration of leptin. Experiments using lean and obese mice will identify alternative candidate TFs that regulate programs underlying obesity.

IRF3 is expressed in most mammalian cells, and some of its transcriptional targets have been identified in macrophages and adipocytes^{27,34,42}. In immune cells, IRF3 is known to drive the expression of interferon beta (*Irfb1*) along with a whole host of interferon-stimulated genes (ISGs), cytokines, and other mediators of the innate antiviral response pathway³⁷. Interestingly, our study revealed that many canonical IRF3 target genes were not detected in AgRP neurons during either of the two states in which we predict IRF3 is active (e.g., fed and leptin-treated), including *Irfb1*, *Isg15*, *Isg54*, *Isg56*, *Ccl4*, *Ccl5*, *Cxcl10*, among others. Thus, IRF3 in AgRP neurons has transcriptional targets that are distinct compared to those found in other cell types. Our ATAC-seq data suggests that this may be due to an underlying chromatin landscape in AgRP neurons that restricts access of IRF3 to classical target genes. It is also possible that specific interacting proteins direct IRF3 to distinct loci in hepatocytes and immune cells vs.

neurons. The IRF3 cistrome has not been determined in any other CNS cell types, and so the generalizability of this phenomenon is unclear, although it should be noted that many transcription factors exhibit different cistromes in different cell types^{57–59}.

It is interesting to speculate why a pro-inflammatory transcription factor might be co-opted for use in energy homeostasis. During illness, such as after viral infection, appetite is generally suppressed, an effect known as the sickness response. Polyinosinic:polycytidylic acid (Poly(I:C)), a synthetic analog of double-stranded RNA and a potent activator of TLR3, has been shown to mimic a viral infection and is able to evoke a classic sickness response, including hypophagia and decreased locomotor activity, when systemically or centrally administered to mice^{31,32}. IRF3 is a dominant transcriptional effector of TLR3 receptor activation³⁷, and it is highly probable that IRF3 mediates the transcriptional programs underlying the prolonged sickness behaviors caused by poly(I:C) treatment or viral infection. It might therefore make sense for evolution to converge on the same pathway as an effector of homeostatic appetite control outside of the context of illness, such as during fasting or feeding.

Our study has certain limitations. First, all of our experiments were performed in male mice, and it is possible that results may differ in females. Second, we used 3 hours-post leptin administration since it had been previously shown that leptin gradually suppresses the firing rate of AgRP neurons over the course of 3 h (Beutler et al., 2017). Thus, we suspected that we would be able to detect discernable transcriptional changes related to the alterations in the firing rate of AgRP neurons following leptin-treatment at this time point. We may be missing transient transcriptional changes in various IEGs, or other transcripts. Third, most of our studies are restricted to AgRP neurons, and it remains to be seen whether IRF3 has a role downstream of leptin signaling in other leptin sensitive cell types. Finally, it is unclear whether our studies inform us about human biology. Variation at the *IRF3* locus has not been associated with body weight in humans, either in GWAS studies or in exome sequencing of patients with extreme obesity. Consistent with this, we have not seen a major effect on body weight in AgI3KO mice. Our data support a role of IRF3 in mediating the acute effects of leptin on AgRP neuronal activity—it's likely that other leptin signaling pathways are more important in chronic weight maintenance.

Methods

Mouse models

Generation of mice. IRF3-2D mice (Jackson Labs Strain #036261) and IRF3 floxed (Jackson Labs Strain #:036260) mouse founder lines were

used³⁴. For loss-of-function studies, we crossed *Irf3*^{fl^{ox}} mice with AgRP-IRES-Cre mice (Jackson Labs Strain #012899)⁴³ to generate AgRP neuron-deficient IRF3 mice (Agl3KO). For gain-of-function studies, we crossed *IRF3*^{2D} mice with AgRP-IRES-Cre mice to generate mice expressing constitutively active IRF3 in their AgRP neurons (Agl3-2D). We crossed transgenic Nuclear tagging and Translating Ribosome Affinity Purification (NuTRAP; Jackson labs Strain #:029899) mice with AgRP-IRES-Cre mice to generate the NuTRAP^{AgRP} mouse line, from which we could isolate AgRP neuron-specific mRNA and nuclei. Male mice, maintained on a C57Bl/6J background, were used for all studies.

Other sources. Global IRF3 knockout (IRF3KO) mice were obtained from the RIKEN BRC Experimental Animal Division (RBRC00858)⁴⁴. C57Bl/6J were purchased from Jackson Labs (WT, Jackson Labs Strain 000664). POMC-IRES-Cre⁴⁵ were gifted by Bradford Lowell (BIDMC and Harvard Medical School).

Animals: standard fed, fasted, and leptin-treated comparison

All animal experiments were performed with approval from the Institutional Animal Care and Use Committees of The Harvard Center for Comparative Medicine and Beth Israel Deaconess Medical Center (IACUC protocol numbers 056-2017, 024-2020, 018-2023). 6-to-11-week-old male C57Bl/6J NuTRAP^{AgRP} mice were fed a standard chow diet *ad libitum*. At least one day before the experiment, mice were singly-housed in a cage with wood chip bedding and handled by the experimenter using a cupping method shown to reduce anxiety in mice⁴⁶. Mice were either maintained on their chow diet (Lab Diet, cat no 5008; fed mice), or fasted (fasted mice) overnight for 18-20 hours. At zeitgeber ZT time 2-4, mice were intraperitoneally (i.p.) injected with either vehicle (PBS) or leptin (5 mg/kg) and euthanized 3 hours later. As described in Campbell et al., 2017, with minor alterations, brains were rapidly extracted, and then placed ventral surface up into a chilled stainless steel brain matrix (catalog no. SA-2165, Roboz Surgical Instrument Co., Gaithersburg, MD) embedded in ice-cold PBS. Using GFP fluorescence to demarcate the ARCs rostral and caudal boundaries, brains were blocked to obtain a single coronal section containing the entire GFP+ arcuate, ~2 mm thick. The ARC was crudely micro-dissected using a surgical blade at its visually approximated dorso-lateral borders and immediately snap frozen on dry ice and stored at -80 °C.

Immunohistochemistry

Immunohistochemistry was performed as described (Campbell et al., 2017) with minor alterations. Mice were terminally anesthetized with 7% chloral hydrate (350 mg/kg) diluted in isotonic saline and transcardially perfused with phosphate-buffered saline (PBS) followed by 10% PFA. Brains were removed, stored in the same fixative overnight, and then transferred into 20% sucrose at 4 °C overnight and cut into 40-µm coronal sections on a freezing microtome.

Brain sections were washed 3 times in PBS for 10 minutes each at room temperature (RT). Sections were then subjected to antigen retrieval first by being pretreated with 1% NaOH and 1% H₂O₂ in H₂O, for 20 minutes. Sections were then treated with 0.3% glycine in H₂O for 10 minutes, followed by incubation with 0.03% sodium dodecyl sulfate for 10 minutes. Sections were then blocked for 1 hour with 3% normal goat serum in PBS/0.25% Triton-X-100. 1:250 rabbit anti-phospho-STAT3 (Tyr705) (D3A7) XP (catalog #9145 S, Cell Signaling) or rabbit anti-IRF3 (catalog #4302 S, Cell Signaling) was then added and incubated overnight at 4 °C. The following day, sections were washed 3 times for 10 min in PBS at RT. Next, sections were treated with Alexa Fluor 647-conjugated donkey anti-rabbit (for pSTAT3 experiments, diluted 1:1000; catalog no. A-31573, Thermo Fisher Scientific) for 2 h in the dark at RT. Sections were washed three times in PBS, mounted onto gelatin-coated slides (Southern Biotech), cover slipped with Vectashield Anti-fade Mounting Medium with DAPI (Vector Labs,

Burlingame, CA) and sealed with nail polish. Fluorescence images were captured with an Olympus VS120 slide scanner microscope and with a confocal microscope (Zeiss LSM510 Upright Confocal System).

Real-time PCR analysis

Cells or tissues were collected in Trizol reagent (Thermo Fisher), and tissues were mechanically homogenized using the TissueLyser II bead-mill (Qiagen). Total RNA was isolated using E.Z.N.A. Total RNA Kit II (Omega Bio-Tek) based on the manufacturer's protocol. Up to 1 µg RNA was reverse-transcribed using the High-Capacity cDNA Reverse Transcription Kit (Thermo Fisher Scientific). Using 0.5 ng cDNA in a commercial SYBR Green PCR Master Mix (Thermo Fisher Scientific) and specific gene primers (see Supplementary Table 1), qRT-PCR was performed on the QuantStudio 6 Flex Real-Time PCR System (Thermo Fisher Scientific) and normalized to the housekeeping gene *Hprt* for murine studies. Analysis of qPCR data was conducted via the 2^{-ΔΔCT} method⁴⁷.

Translating ribosome affinity purification (TRAP) immunoprecipitation (IP)

TRAP IP was performed as previously described (Roh et al., 2017). Briefly, for each sample 4 frozen ARC tissue samples from NuTRAP^{AgRP} mice between 6 and 11 weeks of age were pooled and lysed with Dounce homogenizers in low-salt IP buffer (50 mM Tris [pH7.5], 12 mM MgCl₂, 100 mM KCl, 1% NP-40; 100 µg/ml cycloheximide, 2 mM DTT, 0.2 units/ml RNasin, 1x Roche Complete EDTA-free protease inhibitor). After centrifugation, the supernatant was incubated with GFP ab290 antibody (Abcam) on a rotor, then incubated again with Dynabeads Protein G (Thermo Fisher). An internal control was also collected from the lipid-free supernatant prior to antibody incubation. The TRAP portion of the protocol took ~1.5 hours and RNase-inhibitors were used throughout the protocol to mitigate potential RNA degradation. RNA was isolated with the RNeasy Micro Kit (Qiagen) according to manufacturer's instructions, and then reverse-transcribed and analyzed by qRT-PCR as described above. TRAP-isolated RNA (<100 ng) was treated with the Ribo-Zero rRNA removal kit (Epicentre) to deplete ribosomal RNA and converted into double stranded cDNA using NEBNext mRNA Second Strand Synthesis Module (E6111L). cDNA was subsequently tagmented and amplified for 12 cycles by using Nextera XT DNA Library Preparation Kit (Illumina FC-131). Sequencing libraries were analyzed by Qubit and Agilent Bioanalyzer, pooled at a final concentration of 12pM, and sequenced on a NextSeq500.

RNA-seq analysis

RNA-seq data was aligned using HISAT2 (Kim et al., 2015). Reads were assigned to genes using feature Counts and a GRCm38 genome modified to minimize overlapping transcripts (Liao et al., 2014). Differential expression analysis of the data was performed with edgeR using a quasi-likelihood GLM fitted to the "treatment"/condition (fed/fasted/leptin) and testing the contrasts between the groups fasted-fed and leptin-fasted using the 'QLFtest' function⁴⁸. Significantly different genes were required to have an average expression, across group, of > 1 cpm, a fold change (FC) > 0.5, an adjusted p-value, false discovery rate (fdr), value of <0.05. Gene set enrichment analysis (GSEA) gene ontology (GO) for biological process was carried out with WebGestalt (WEB-based GENE SeT Analysis Toolkit)⁴⁹. Genes with cpm <1 were omitted from the GSEA analysis.

Isolation of AgRP neuronal nuclei from NuTRAP Mice

AgRP neuronal nuclei were isolated as previously described (Roh et al., 2017), with minor alterations. Briefly, dissected ARCs from 6-11-week-old mice were snap frozen and stored at -80C. Isolated ARCs were dounce homogenized in nuclear preparation buffer (NPB; 10 mM HEPES [pH 7.5], 1.5 mM MgCl₂, 10 mM KCl, 250 mM sucrose, 0.1% NP-40, and 0.2 mM DTT), and homogenates were filtered through a

100 μM strainer and centrifuged to pellet the nuclei. Nuclei were washed with NPB, re-suspended in nuclear sorting buffer (10 mM Tris [pH 7.5], 40 mM NaCl, 90 mM KCl, 2 mM EDTA, 0.5 mM EGTA, 0.1% NP-40, 0.2 mM DTT), and filtered again through a 40 μM strainer. Isolated nuclei were sorted by flow cytometry based on AgRP neuron-specific GFP expression. With this approach we routinely obtain ~2000 AgRP neuronal nuclei per mouse.

Nuclei processing and library preparation for ATAC-seq

NuTRAP^{AgRP} ARC nuclei from 4 pooled mice, per samples, were isolated, subjected to FANS, and 10,000 nuclei were collected into 500–750 μL PBS (0.1% NP40) in 1.5 mL microcentrifuge tubes and stored on ice. Two biological replicates, of 10,000 nuclei each, were used for each experimental condition. Tubes were spun at 1000 rpm for 10 mins, at 4 °C. Supernatant was removed via gentle decantation. Nuclei pellets were subjected to tagmentation after resuspension in 50 μL of transposase reaction mix: 25 μL TD buffer, 2.5 μL TN5 transposase, 22.5 μL dH₂O. Nuclei were incubated at 37 °C with shaking at 600 rpm for 30 mins, then placed on ice. DNA was purified using a Qiagen minelute PCR purification kit and eluted in 10 μL of Qiagen Elution Buffer. Library construction was conducted using an initial PCR amplification using 10 μL of transposed DNA, 11 μL H₂O, 2 μL of 25 μM Primer 1, 2 μL of Primer 2, and 25 μL of NEBNext HF 2X PCR mix. The following initial amplification cycle was used: 1 cycle of 72 °C (5 min), 98 °C (30 s), 5 cycles of 98 °C (10 s), 63 °C (30 s), 72 °C (1 min), hold at 4 °C. A side PCR reaction was conducted to determine the optimal number of amplification cycles used during the library construction, as previously described⁵⁰. Briefly, the side PCR reaction was performed using 5 μL PCR amplified DNA, 4.41 μL H₂O, 0.25 μL Primer 1 Adapter, 0.25 μL Primer 2 Adapter 2 (barcoded), 0.09 μL 100x SYBR Green (Diluted from 10,000X stock with H₂O), 5 μL NEBNext HF 2X PCR mix. The following initial amplification cycle was used: 1 cycle of 98 °C (30 s), 20 cycles of 98 °C (10 s), 63 °C (30 s), 72 °C (1 min). Cycle vs. Linear Rn was plotted, the maximal fluorescence intensity (Rn) was determined, and the closest cycle # that produced the 1/3 Max Rn value was used to determine the additional cycles needed during library construction⁵⁰. The required additional number of cycles (6 for all libraries) was completed by adding the sample back to the thermocycler in its same tube and master mix. Amplified libraries were purified with a Qiagen Minilute PCR purification kit, eluted in 20 μL , and the volume was brought up to 100 μL with additional EB. The eluent was subjected to a two-phase size selection using Ampure Beads, initially .55X volume of elutant (55 μL) was used, followed by 1.5X volume of initial sample volume (100 μL \times 1.5 = 150 μL) minus the existing PEG that is already in the sample (150 μL – 55 μL = 95 μL). Finally, the library was eluted using 50 μL of EB. Libraries were sequenced on a Next-seq 500 (Illumina).

ATAC-seq data processing

Library reads were mapped to the UCSC build mm10 assembly of the mouse genome using Bowtie2, with peak calling using MACS2. ATAC-seq peaks were visualized in the WashU Epigenome Browser. Coverage summation and additional data parsing were carried out using Bedtools. Differential binding analysis, including normalization and quantification, was done in edgeR. Differential peaks were defined at log₂ fold change \geq 0.5 and a false discovery rate of $<$ 0.05. ATAC-seq peaks with a CPM $<$ 1 were excluded from the differential analysis.

Motif enrichment analysis and TF prioritization

Transcriptionally concordant ATAC-seq peaks were subjected to Motif Enrichment was determined using the MEME-suite Analysis of Motif Enrichment (AME) (Version 5.1.0) sequence analysis tool (Fig. 3a)²⁴. We restricted our analysis to significant concordant peaks for each of the four significant ATAC-seq peak patterns (i.e., fasted-opened, fasted-closed, leptin opened, leptin-closed); genes without an annotated TSS

were removed from our analysis. AME was conducted 6 distinct times using one of the 6 possible background control sets of peaks during each analysis: (1) neutral (i.e., unchanging) peaks anywhere in the genome; (2) neutral peaks near neutral genes; (3) neutral peaks near significant genes; (4) neutral peaks near any TSS; (5) all non-concordant ATAC-seq peaks for a given conditions (e.g., leptin-opened); or (6) concordant ATAC-seq peaks that are shuffled (e.g., leptin-opened peak sequences that are shuffled). Thus, in all, 6 distinct instances of AME were performed for each peak set. We next employed a rule whereby we further considered motifs only if they were significantly enriched in \geq 5 out of 6 AME instances (Fig. S3a, e).

For AME analysis, p -value is the optimal enrichment p -value of the motif according to the statistical test, adjusted for multiple tests using a Bonferroni correction. To determine the representative log transformed p -values (for plotting purposes), for those “enriched” motifs (at least 5 out of 6 AME instances), the minimal (most significant) p -value out of the 6 motif instances was determined, while omitting from the analysis any non-significant p -values, for those Motifs that have a single non-significant motif but are retained. Conversely, to determine the representative p -value for those non-enriched motifs (violate the at least 5 out of 6 significant rule) we calculated the minimal (most significant) p -value, of the non-significant ones. We then log-transformed the resulting p values (log₂). For the transcriptionally concordant fasted-opened condition only, p -values for 12 of the 356 TF motifs were less than e^{-300} and thus could not be log transformed (ATF3.O.A, BACH1.O.C, BACH2.O.A, BATF.O.A, CRX.O.A, FOS.O.A, FOSB.O.A, FOSL1.O.A, FOSL2.O.A, JUN.O.A, JUNB.O.A, JUND.O.A). Therefore, for these motifs, only in fasted-opened condition, the log transformed p -value was determined by imputation. Evidently, none of these 12 TF motifs were qualified (due to enrichment in disqualifying chromatin conditions) to be plotted in Fig. 3g or i. All plots were made using Graphpad PRISM software (Version 9).

In vitro leptin-induced pSTAT3 measurement experiments

Immortalized hypothalamic GT1-7 cells³⁷ were plated in DMEM with high glucose (Sigma, D5796), Penicillin-Streptomycin, and 10% fetal bovine serum. Cells were transiently transfected using Lipofectamine 3000 Reagent (Thermo Fisher) based on manufacturer’s instructions. Briefly, dsDNA-lipid complexes were prepared using 0.5 μg of plasmid expressing the murine long-form leptin receptor (OB-Rb; LepR)⁵¹, or both LepR plasmid and the GFP-tagged IRF3 plasmid, and Lipofectamine 3000 with P1000 reagent in Opti-MEM Medium (Thermo Fisher), and then added dropwise onto cells in medium. Cells were washed with PBS, treated with serum-free DMEM, and treated with either leptin (100 nM) or vehicle (control) for 15 minutes.

Immunoblotting

Lysis of frozen tissue was performed in 1X RIPA lysis buffer (Millipore Sigma) with the addition of protease and phosphatase inhibitors (Millipore Sigma). Tissues were mechanically homogenized using the TissueLyser II bead-mill (Qiagen). Total protein was quantified via BCA Protein Assay Kit (Thermo Scientific), protein lysate was prepared in 1X SDS in RIPA lysis buffer, and then boiled. Lysis of cells was performed as previously described (Silva et al., 2018). Briefly, media was aspirated from plated cells, and then 1X SDS in RIPA lysis buffer was added onto the cells, which were then collected, flash frozen, and boiled. The prepared protein samples were separated on Tris-HCl protein gels (Bio-Rad) and transferred to PVDF membranes (Thermo Fisher), followed by blocking in 5% blotting-grade milk (Bio-Rad). Blots were incubated in appropriate primary antibodies (1:1000 dilution unless otherwise indicated) at 4 °C overnight, and then in secondary HRP-conjugated antibody (Cytiva) for one hour at RT. Blots were developed with chemiluminescent ECL reagents (Thermo Fisher) and imaged with ImageLab™ Touch Software (Bio-Rad) on the ChemiDoc Touch Imaging System (Bio-Rad).

In vitro IRF3 live-cell imaging and quantification

80,000 GT1-7 cells were plated in two wells of an 8-well Nunc™ Lab-Tek™ II Chambered Coverglass (Catalog # 155360) in media. The following day cells were transfected with plasmids expressing mouse LepR (OB-Rb)⁵¹ and IRF-GFP, as described above. The following afternoon, cells were washed with 37 °C PBS and serum-free DMEM (Sigma #D1145) was added to cells prior to imaging approximately 1 hour later. Ideal cells, for which the nucleus was well demarcated, and for which the IRF3-GFP expression was apparent, were targeted and images were scanned and recorded every 10 minutes obtained using a Zeiss LSM 880 upright laser scanning confocal microscope in 3 × 3 tile-scan mode with a Plan-Apochromat 20×/0.8 M27 objective. Given the absence of a nuclear dye in this experiment, the nuclear domain was demarcated based on the clear contrast between cytoplasm and nucleus present at the 3-hour time point. Mean Fluorescence Intensity of each targeted cell's cytoplasm and nuclei was determined using ImageJ software (NIH) to enable calculation of the nuclear-to-cytoplasm (N/C) GFP intensity ratio.

Flow cytometry to measure nuclear IRF3 in vivo

6-to-11-week-old male C57BL/6J male mice were maintained on a standard chow diet *ad libitum*. Mice were handled for 5-minutes on the days prior to the experiment. Mice were fasted overnight for 19 h, before being injected I.P. with leptin (5 mg/kg). Using a modified version of the FAST-FIN protocol⁵², 5 h later, mice were rapidly perfused with 10% formalin for 1-minute, and whole hypothalami were isolated and snap-frozen in a microcentrifuge tube on dry ice. Whole mouse hypothalamus was rapidly isolated 5 h later. Later, individual mouse hypothalami were subjected to dounce homogenization and immediately fixed using 1% formaldehyde for 7-minutes at RT, followed by quenching with 125 mM glycine for 5-minutes. Nuclei were collected and resuspended in 22% OptiPrep which was layered on top of a 43% Optiprep, and centrifuged at 10,000 g for 30-minutes. Nuclei were resuspended with Blocking Buffer (without Triton-X, in PBS) and centrifuged for 10,000 g for 10 min at 4 °C. Supernatant was removed and replaced with 500 ul premade Blocking Buffer with Triton-X in PBS and nuclei were blocked for 10 min at RT. Antibody was added (IRF3, 1:250; pSTAT3, 1:250) and incubated for 1-hour. Nuclei were washed with 1X wash buffer with triton-X, resuspended in Blocking Buffer with triton-X, and incubated with 1:500 secondary antibody (Alexa Fluor 647 Donkey anti-rabbit IgG) for 30-minutes at RT while light protected. Nuclei were then spun down (600 g for 3-minutes at 4 °C) and gently resuspended in 500 ul FACS buffer with Iul Hoechst, while in a 5 mL round-bottom FACS tube and ran on the CytoFLEX LX.

Fasting-refeeding studies

In this study, 6-to-11-week-old male C57BL/6J NuTRAP^{AgRP} male mice were fed standard chow diet *ad libitum*. At least one day before the experiment, mice were singly housed and handled by the experimenter using a cupping method shown to reduce anxiety⁴⁶. Depending on the experiment, mice were fasted overnight starting at ZT 8-10. The following day, between ZT 3-5, mice were injected i.p. with leptin, and 30 minutes later a weighed food grate was given. Food was measured during a 24-hour period. For the Ag13KO fasting-refeeding experiment, a white paper mesh (Alpha pads) was added to the cage in place of bedding, to allow for the accounting of spilled food when calculating food intake. Food intake was obtained by subtracting remaining food, including any spilled food in cages, from the previously weighed food amount⁵³. Food intake adjusted for body weight was calculated by dividing the absolute food intake by body weight and multiplying the result by the average body weight of all mice⁵⁴.

Telemetry experiments

All surgeries were performed in sterile conditions. Mice were anesthetized with a mix of ketamine/xylazine (100 and 10 mg/kg,

respectively, IP) with additional doses of 10% of the initial dose throughout surgery to eliminate the withdrawal reflex. Mice were implanted with a radiotelemetry temperature and locomotion sensor (TA-F10, DSI) in the intraperitoneal space via laparotomy⁵⁵. Meloxicam treatment, for analgesia, was administered prior to surgery, and then again 24hrs later. Mice were allowed to recover at least 10 days prior to experimentation. Following recovery, mice used for experiments showed no signs of discomfort and gained weight normally⁵⁵. Core body temperature and locomotion were recorded using the radiotelemetry DSI system. The signal was sent from the telemetry probes previously implanted to receivers and converted using the PhysioTel HD and PhysioTel (DSI) hardware, which provides the mean of Tc every 5 min. All animals had at least 48 hours of acclimation in the recording chamber before the baseline was recorded. To account for occasional technical artifacts associated with continuously recording core body temperature, those 5-min interval average LMA scores that were more or less than the grand average LMA score (across all mice, conditions, and time points) plus or minus 2 times the standard deviation (i.e., $36.897 \pm (2 * 2.316)$), were omitted (e.g., greater than 41.5°C and less than 32.3°C). Two Ag13KO mice were removed from the leptin-treat phase of the experiment, due to their cannula being damaged, and rendered unusable, during the final leptin-treatment phase of the experiment.

General In vivo Stereotaxic Injections

Mice were anesthetized with xylazine (10 mg/kg, i.p.) and ketamine (100 mg/kg, i.p.) and placed in a stereotaxic apparatus after assuring proper anesthesia effects with a toe pinch or tail pull. The fur around the skull was shaved and the skin sanitized. An incision in the skin overlying the skull was made and the skull surface exposed. A small hole was then drilled into the skull to expose the brain surface. The ARC was bilaterally localized according to the coordinates listed in mouse brain in stereotaxic coordinates by Paxinos⁵⁶ and the tip of the nanoject injector connected to a sterile glass pipette was lowered into the ARC bilaterally (coordinates for ARC injections were anterior -1.37 mm, lateral \pm 0.3 mm, and ventral 5.70-5.80). pAAV-hSyn-DIO-H2B-mCherry (Addgene plasmid # 50459), was then slowly injected. Afterwards, the edges of the incision were reapposed with tissue adhesive (vetbond, n-butyl cyanoacrylate). Analgesia was given in the form of Meloxicam SR (4 mg/kg). Animals were allowed to recover from surgery for 2 weeks and their body weight and health conditions were closely monitored during recovery. Coordinates and injection volume used in the studies were: the ARC (anterior-posterior (AP): -1.40 mm, dorsal-ventral (DV): -5.80 mm, left-right (LR): \pm 0.30 mm, 150 nl/side). Accuracy of injection was determined by the expression of mCherry driven by AgRP-IRES-Cre exclusively within the ARC, both during tissue collection and during FACS.

Quantification and statistical analysis

Sample size, mean, and significance P values are indicated in the text, figure legends, or Method Details. Error bars in the experiments represent standard deviation (STD) from either independent experiments or independent samples. Statistical analyzes were performed using GraphPad Prism. Detailed information about statistical methods is specified in figure legends or Method Details.

Reporting summary

Further information on research design is available in the Nature Portfolio Reporting Summary linked to this article.

Data availability

All raw and processed RNA-Seq and ATAC-seq data has been deposited in the NCBI Gene Expression Omnibus (GEO) and assigned an accession number GEO: [GSE240484](https://www.ncbi.nlm.nih.gov/geo/query/acc.cgi?acc=GSE240484). The reference genome used for RNA-

Seq and ATAC-seq raw sequencing read alignment is mm10. Source data are provided with this paper.

Code availability

All scripts used in the current study are available on Zenodo [<https://doi.org/10.5281/zenodo.10967242>], the used packages are listed in the Methods session.

References

- Andermann, M. L. & Lowell, B. B. Toward a wiring diagram understanding of appetite control. *Neuron* **95**, 757–778 (2017).
- Luquet, S., Perez, F. A., Hnasko, T. S. & Palmiter, R. D. NPY/AgRP neurons are essential for feeding in adult mice but can be ablated in neonates. *Science* **310**, 683–685 (2005).
- Beutler, L. R. et al. Dynamics of gut-brain communication underlying hunger. *Neuron* **96**, 461–475.e5 (2017).
- Xu, J. et al. Genetic identification of leptin neural circuits in energy and glucose homeostases. *Nature* **556**, 505–509 (2018).
- Henry, F. E., Sugino, K., Tozer, A., Branco, T. & Sternson, S. M. Cell type-specific transcriptomics of hypothalamic energy-sensing neuron responses to weight-loss. *Elife* **4**, e09800 (2015).
- Hummel, K. P., Dickie, M. M. & Coleman, D. L. Diabetes, a new mutation in the mouse. *Science* **153**, 1127–1128 (1966).
- Gao, Q. et al. Disruption of neural signal transducer and activator of transcription 3 causes obesity, diabetes, infertility, and thermal dysregulation. *Proc. Natl Acad. Sci. USA* **101**, 4661–4666 (2004).
- Bates, S. H. et al. STAT3 signalling is required for leptin regulation of energy balance but not reproduction. *Nature* **421**, 856–859 (2003).
- Gong, L. et al. Signal transducer and activator of transcription-3 is required in hypothalamic agouti-related protein/neuropeptide y neurons for normal energy homeostasis. *Endocrinology* **149**, 3346–3354 (2008).
- Allison, M. B. et al. Defining the transcriptional targets of leptin reveals a role for Atf3 in leptin action. *Diabetes* **67**, 1093–1104 (2018).
- Campbell, J. N. et al. A molecular census of arcuate hypothalamus and median eminence cell types. *Nat. Neurosci.* **20**, 484–496 (2017).
- Cedernaes, J. et al. Transcriptional basis for rhythmic control of hunger and metabolism within the agrp neuron. *Cell Metab.* **29**, 1078–1091.e5 (2019).
- Inoue, F. et al. Genomic and epigenomic mapping of leptin-responsive neuronal populations involved in body weight regulation. *Nat. Metab.* **1**, 475–484 (2019).
- Mikkelsen, T. S. et al. Comparative epigenomic analysis of murine and human adipogenesis. *Cell* **143**, 156–169 (2010).
- Hiraiki, Y. et al. NFIA co-localizes with PPAR γ and transcriptionally controls the brown fat gene program. *Nat. Cell Biol.* **19**, 1081–1092 (2017).
- Su, Y. et al. Neuronal activity modifies the chromatin accessibility landscape in the adult brain. *Nat. Neurosci.* **20**, 476–483 (2017).
- Guan, D. et al. The hepatocyte clock and feeding control chronophysiology of multiple liver cell types. *Science* **369**, 1388–1394 (2020).
- Stroud, H. et al. An activity-mediated transition in transcription in early postnatal neurons. *Neuron* **107**, 874–890.e8 (2020).
- Betley, J. N., Cao, Z. F. H., Ritola, K. D. & Sternson, S. M. Parallel, redundant circuit organization for homeostatic control of feeding behavior. *Cell* **155**, 1337–1350 (2013).
- Roh, H. C. et al. Warming induces significant reprogramming of beige, but not brown, adipocyte cellular identity. *Cell Metab.* **27**, 1121–1137.e5 (2018).
- Hael, C. E., Rojo, D., Orquera, D. P., Low, M. J. & Rubinstein, M. The transcriptional regulator PRDM12 is critical for Pomc expression in the mouse hypothalamus and controlling food intake, adiposity, and body weight. *Mol. Metab.* **34**, 43–53 (2020).
- Takahashi, K. A. & Cone, R. D. Fasting induces a large, leptin-dependent increase in the intrinsic action potential frequency of orexigenic arcuate nucleus neuropeptide y/agouti-related protein neurons. *Endocrinology* **146**, 1043–1047 (2005).
- Ahima, R. S. et al. Role of leptin in the neuroendocrine response to fasting. *Nature* **382**, 250–252 (1996).
- Bailey, T. L., Johnson, J., Grant, C. E. & Noble, W. S. The MEME suite. *Nucleic Acids Res* **43**, W39–W49 (2015).
- Yap, E.-L. & Greenberg, M. E. Activity-regulated transcription: bridging the gap between neural activity and behavior. *Neuron* **100**, 330–348 (2018).
- Eguchi, J. et al. Transcriptional control of adipose lipid handling by IRF4. *Cell Metab.* **13**, 249–259 (2011).
- Kumari, M. et al. IRF3 promotes adipose inflammation and insulin resistance and represses browning. *J. Clin. Invest* **126**, 2839–2854 (2016).
- Fitzgerald, K. A. et al. IKKepsilon and TBK1 are essential components of the IRF3 signaling pathway. *Nat. Immunol.* **4**, 491–496 (2003).
- Huang, H. et al. Rho-kinase regulates energy balance by targeting hypothalamic leptin receptor signaling. *Nat. Neurosci.* **15**, 1391–1398 (2012).
- Hirata, Y., Broquet, A. H., Menchén, L. & Kagnoff, M. F. Activation of innate immune defense mechanisms by signaling through rig-i/ips-1 in intestinal epithelial cells. *J. Immunol.* **179**, 5425–5432 (2007).
- Cunningham, C., Campion, S., Teeling, J., Felton, L. & Perry, V. H. The sickness behaviour and CNS inflammatory mediator profile induced by systemic challenge of mice with synthetic double-stranded RNA (poly I:C). *Brain Behav. Immun.* **21**, 490–502 (2007).
- Zhu, X., Levasseur, P. R., Michaelis, K. A., Burfeind, K. G. & Marks, D. L. A distinct brain pathway links viral RNA exposure to sickness behavior. *Sci. Rep. -uk* **6**, 29885 (2016).
- Luheshi, G. N., Gardner, J. D., Rushforth, D. A., Loudon, A. S. & Rothwell, N. J. Leptin actions on food intake and body temperature are mediated by IL-1. *Proc. Natl Acad. Sci. USA* **96**, 7047–7052 (1999).
- Yan, S. et al. IRF3 reduces adipose thermogenesis via ISG15-mediated reprogramming of glycolysis. *J. Clin. Invest.* **131**, e144888 (2021).
- Harris, R. B. S. Phosphorylation of STAT3 in hypothalamic nuclei is stimulated by lower doses of leptin than are needed to inhibit food intake. *Am. J. Physiol. -endoc M* **321**, E190–E201 (2021).
- Barnes, T. M. et al. Identification of the leptin receptor sequences crucial for the STAT3-Independent control of metabolism. *Mol. Metab.* **32**, 168–175 (2020).
- Antonczyk, A. et al. Direct inhibition of irf-dependent transcriptional regulatory mechanisms associated with disease. *Front Immunol.* **10**, 1176 (2019).
- Shu, C., Li, X. & Li, P. The mechanism of double-stranded DNA sensing through the cGAS-STING pathway. *Cytokine Growth F. R.* **25**, 641–648 (2014).
- Joung, S. M. et al. Akt contributes to activation of the trif-dependent signaling pathways of tlrs by interacting with tank-binding kinase 1. *J. Immunol.* **186**, 499–507 (2011).
- Yeon, S. H., Song, M. J., Kang, H. & Lee, J. Y. Phosphatidylinositol-3-kinase and Akt are required for RIG-I-mediated anti-viral signalling through cross-talk with IPS-1. *Immunology* **144**, 312–320 (2015).
- Wall, Evande et al. Collective and individual functions of leptin receptor modulated neurons controlling metabolism and ingestion. *Endocrinology* **149**, 1773–1785 (2008).
- Ourthiague, D. R. et al. Limited specificity of IRF3 and ISGF3 in the transcriptional innate-immune response to double-stranded RNA. *J. Leukoc. Biol.* **98**, 119–128 (2015).

43. Tong, Q., Ye, C.-P., Jones, J. E., Elmquist, J. K. & Lowell, B. B. Synaptic release of GABA by AgRP neurons is required for normal regulation of energy balance. *Nat. Neurosci.* **11**, 998–1000 (2008).
44. Sato, M. et al. Distinct and essential roles of transcription factors *irf-3* and *irf-7* in response to viruses for *irf- α / β* gene induction. *Immunity* **13**, 539–548 (2000).
45. Fenselau, H. et al. A rapidly acting glutamatergic ARC \rightarrow PVH satiety circuit postsynaptically regulated by α -MSH. *Nat. Neurosci.* **20**, 42–51 (2017).
46. Hurst, J. L. & West, R. S. Taming anxiety in laboratory mice. *Nat. Methods* **7**, 825–826 (2010).
47. Livak, K. J. & Schmittgen, T. D. Analysis of relative gene expression data using real-time quantitative pcr and the $2^{-\Delta\Delta c t}$ method. *Methods* **25**, 402–408 (2001).
48. Robinson, M. D., McCarthy, D. J. & Smyth, G. K. edgeR: a Bioconductor package for differential expression analysis of digital gene expression data. *Bioinformatics* **26**, 139–140 (2010).
49. Wang, J., Vasaikar, S., Shi, Z., Greer, M. & Zhang, B. WebGestalt 2017: a more comprehensive, powerful, flexible and interactive gene set enrichment analysis toolkit. *Nucleic Acids Res* **45**, W130–W137 (2017).
50. Buenrostro, J. D., Wu, B., Chang, H. Y. & Greenleaf, W. J. ATAC-seq: A Method for Assaying Chromatin Accessibility Genome-Wide. *Curr. Protoc. Mol. Biol.* **109**, 21.29.1–21.29.9 (2015).
51. Chen, Y. et al. Enhancement of hypothalamic stat3 acetylation by nuclear receptor *nur77* dictates leptin sensitivity. *Diabetes* **64**, 2069–2081 (2015).
52. Marion-Poll, L., Montalban, E., Munier, A., Hervé, D. & Girault, J. Fluorescence-activated sorting of fixed nuclei: a general method for studying nuclei from specific cell populations that preserves post-translational modifications. *Eur. J. Neurosci.* **39**, 1234–1244 (2014).
53. Yang, Y., Smith, D. L., Keating, K. D., Allison, D. B. & Nagy, T. R. Variations in body weight, food intake and body composition after long-term high-fat diet feeding in C57BL/6J Mice. *Obes. Silver Spring Md* **22**, 2147–2155 (2014).
54. Bachmanov, A. A., Reed, D. R., Beauchamp, G. K. & Tordoff, M. G. Food intake, water intake, and drinking spout side preference of 28 mouse strains. *Behav. Genet* **32**, 435–443 (2002).
55. Machado, N. L. S. et al. A glutamatergic hypothalamomedullary circuit mediates thermogenesis, but not heat conservation, during stress-induced hyperthermia. *Curr. Biol.* **28**, 2291–2301.e5 (2018).
56. Kongsman, J.-P. The mouse brain in stereotaxic coordinates Second Edition (Deluxe) By Paxinos G. and Franklin, K.B.J., Academic Press, New York, 2001, ISBN 0-12-547637-X. *Psychoneuroendocrino* **28**, 827–828 (2003).

Acknowledgements

This work was supported by an NIH 3 T32 DK 7516-32 to F.D.H., American Heart Association Postdoctoral Fellowship 18POST33990061 to F.D.H., American Diabetes Association Minority Postdoctoral Fellowship 1-19-PMF-008 to F.D.H., a Burroughs Wellcome Fund Postdoctoral Enrichment Program (PDEP) grant to F.D.H., a Nutrition and Obesity Research Center of Harvard (NORCH, # DK 040561) URM Pilot and Feasibility Grant to F.D.H., a Boston Nutrition and Obesity Research Center URM Pilot and Feasibility Grant to F.D.H., a Brain and Behavior Research Foundation Young Investigator Award to F.D.H., a Simons Foundation Simons Collaboration on Plasticity and the Aging Brain salary supplement provided to F.D.H., and R01 DK085171, R01 DK102173, R01 DK102170, and R01 DK1113669 to E.D.R. We thank the BNORC Functional Genomics and Bioinformatics Core, the BIDMC Flow Cytometry Core, the BIDMC

Confocal Imaging Core, and the Molecular Biology Core Facilities (DFCI). We thank Young-Bum Kim (BIDMC) and Won-Mo Yang (BIDMC) for providing GT1-7 cells and LepR (OB-Rb) plasmid. We thank Bradford Lowell (BIDMC; HMS) and Clifford Saper (BIDMC; HMS) for their helpful comments regarding this manuscript.

Author contributions

F.D.H. conceived this study and interpreted the results of all experiments. E.D.R. supervised this study. F.D.H. optimized, designed, and executed TRAP-seq experiments. F.D.H. and E.D.R. conceived of ATAC-seq studies, which F.D.H. optimized, designed, and executed with advice from E.D.R. and L.T. C.J., R.L., and H.S., performed computational and bioinformatic analyses involving sequencing data. F.D.H. conceived of motif filtering/prioritization scheme. C.J. and F.D.H. curated RNA-seq, ATAC-seq, and Motif enrichment analyzes. F.D.H. performed data visualization for all experiments. F.D.H. conceived of, designed, and executed in vitro, live-cell imaging, and western blot experiments. N.L., F.D.H., and S.J.P. conducted in vitro and in vivo IRF3 antibody optimizations. F.D.H. optimized, designed, and executed all in vivo immunofluorescence experiments. F.D.H., N.M., and A.U. designed and executed telemetry experiments. A.G. and T.S. assisted with animal studies. F.D.H. wrote the manuscript with major input from E.D.R. along with added input from other authors.

Competing interests

The authors declare no competing interests.

Additional information

Supplementary information The online version contains supplementary material available at <https://doi.org/10.1038/s41467-024-48885-y>.

Correspondence and requests for materials should be addressed to Frankie D. Heyward or Evan D. Rosen.

Peer review information *Nature Communications* thanks Jessica Tollkuhn and the other, anonymous, reviewers for their contribution to the peer review of this work. A peer review file is available.

Reprints and permissions information is available at <http://www.nature.com/reprints>

Publisher's note Springer Nature remains neutral with regard to jurisdictional claims in published maps and institutional affiliations.

Open Access This article is licensed under a Creative Commons Attribution 4.0 International License, which permits use, sharing, adaptation, distribution and reproduction in any medium or format, as long as you give appropriate credit to the original author(s) and the source, provide a link to the Creative Commons licence, and indicate if changes were made. The images or other third party material in this article are included in the article's Creative Commons licence, unless indicated otherwise in a credit line to the material. If material is not included in the article's Creative Commons licence and your intended use is not permitted by statutory regulation or exceeds the permitted use, you will need to obtain permission directly from the copyright holder. To view a copy of this licence, visit <http://creativecommons.org/licenses/by/4.0/>.

© The Author(s) 2024